Three-Dimensional Eye-Head Coordination During Gaze Saccades in the Primate

J. DOUGLAS CRAWFORD,[1] MELIKE Z. CEYLAN,[1] ELIANA M. KLIER,[1] AND DANIEL GUITTON[2]
[1]*Centre for Vision Research and Departments of Psychology and Biology, York University, Toronto, Ontario M3J 1P3; and*
[2]*Montreal Neurological Institute and Department of Neurology and Neurosurgery, McGill University, Montreal, Quebec H3A 2B4, Canada*

Crawford, J. Douglas, Melike Z. Ceylan, Eliana M. Klier, and Daniel Guitton. Three-dimensional eye-head coordination during gaze saccades in the primate. *J. Neurophysiol.* 81: 1760–1782, 1999. The purpose of this investigation was to describe the neural constraints on three-dimensional (3-D) orientations of the eye in space (Es), head in space (Hs), and eye in head (Eh) during visual fixations in the monkey and the control strategies used to implement these constraints during head-free gaze saccades. Dual scleral search coil signals were used to compute 3-D orientation quaternions, two-dimensional (2-D) direction vectors, and 3-D angular velocity vectors for both the eye and head in three monkeys during the following visual tasks: radial to/from center, repetitive horizontal, nonrepetitive oblique, random (wide 2-D range), and random with pin-hole goggles. Although 2-D gaze direction (of Es) was controlled more tightly than the contributing 2-D Hs and Eh components, the torsional standard deviation of Es was greater (mean 3.55°) than Hs (3.10°), which in turn was greater than Eh (1.87°) during random fixations. Thus the 3-D Es range appeared to be the byproduct of Hs and Eh constraints, resulting in a pseudoplanar Es range that was twisted (in orthogonal coordinates) like the zero torsion range of Fick coordinates. The Hs fixation range was similarly Fick-like, whereas the Eh fixation range was quasiplanar. The latter Eh range was maintained through exquisite saccade/slow phase coordination, i.e., during each head movement, multiple anticipatory saccades drove the eye torsionally out of the planar range such that subsequent slow phases drove the eye back toward the fixation range. The Fick-like Hs constraint was maintained by the following strategies: first, during purely vertical/horizontal movements, the head rotated about constantly oriented axes that closely resembled physical Fick gimbals, i.e., about head-fixed horizontal axes and space-fixed vertical axes, respectively (although in 1 animal, the latter constraint was relaxed during repetitive horizontal movements, allowing for trajectory optimization). However, during large *oblique* movements, head orientation made transient but dramatic departures from the zero-torsion Fick surface, taking the shortest path between two torsionally eccentric fixation points on the surface. Moreover, in the pin-hole goggle task, the head-orientation range flattened significantly, suggesting a task-dependent default strategy similar to Listing's law. These and previous observations suggest two quasi-independent brain stem circuits: an oculomotor 2-D to 3-D transformation that coordinates anticipatory saccades with slow phases to uphold Listing's law, and a flexible ''Fick operator'' that selects head motor error; both nested within a dynamic gaze feedback loop.

INTRODUCTION

This study deals with the coordinated movements of the eye and head during large gaze shifts, i.e., head-free *gaze saccades*. This topic has been studied with increasing frequency during the last decade, both for its intrinsic importance and as a possible general model for coordination and control. Initial studies focused on one-dimensional (1-D), i.e., horizontal, aspects of eye-head coordination (e.g., Bizzi et al. 1971; Dichgans et al. 1973; Fuller 1996; Guitton 1992; Guitton and Volle 1987; Laurutis and Robinson 1986 Tomlinson 1990) but recently have been extended to two dimensions (Freedman and Sparks 1997; Goossens and Van Opstal 1997). Moreover, the *three-dimensional* (3-D) kinematics of human gaze shifts, i.e., the trajectories of eye and head *orientation* in space, now have been described in some detail (Glenn and Vilis 1992; Misslisch et al. 1998; Radau et al. 1994; Tweed et al. 1995). The latter investigations largely focused on behavioral constraints that reduce the redundant degrees of freedom of the eye-in-space (Es), head-in-space (Hs), and eye-in-head (Eh) during visual fixation. However, it is unclear how the brain organizes 3-D Hs trajectories and coordinates 3-D Eh saccades with vestibuloocular reflex (VOR) slow phases to implement these final fixation constraints. Furthermore, it remains unclear whether these constraints exist to optimize anatomy- or task-related variables (Radau et al. 1994). Finally, an animal model is required to investigate the physiological mechanisms of these behaviors. The purpose of the current investigation was to develop such a model by describing the 3-D kinematic constraints on eye-head coordination during visual fixation in the *monkey*, to determine how the trajectories of the eye and head are controlled to achieve these constraints, and to determine if these constraints optimize anatomic or behavioral requirements.

If the primary purpose of the head-free saccade generator is to redirect gaze direction (i.e., the visual axis in space), then its secondary purpose is probably to determine the 3-D orientation of the eye about this axis. This orientation is important because it determines the geometric correspondence of lines in space with the eye and thus the pattern of retinal stimulation (Crawford and Guitton 1997a; Glenn and Vilis 1992; Haustein and Mittelstaedt 1990; von Helmholtz 1925; Klier and Crawford 1998). In general, Donders' law predicts that the eye will achieve the same orientation for each gaze direction, irrespective of the preceding trajectory (Donders 1848). When the head is mechanically fixed or at rest, a specific form of Donders' law called *Listing's law* is obeyed (Ferman et al. 1987a; von Helmholtz 1925; Tweed and Vilis 1990). Listing's law states that 3-D eye position vectors (defined in the following text) align within a plane such that rotations about a head-fixed

The costs of publication of this article were defrayed in part by the payment of page charges. The article must therefore be hereby marked ''*advertisement*'' in accordance with 18 U.S.C. Section 1734 solely to indicate this fact.

torsional axis are minimized. The question thus arises, does Listing's law continue to hold for Es when the head is free to move?

It appears that when the *human* head is free to move, Donders' law of Es still is obeyed, at least approximately (Straumann et al. 1991). However, the orientations of Es do not form a Listing's plane but rather a twisted 2-D surface (Glenn and Vilis 1992; Radau et al. 1994). The observed twist is more consistent with the orientations produced by a Fick gimbal (e.g., like a telescope mount), where ideally, horizontal movements are achieved through rotations about a body or space-fixed vertical axis, but vertical rotations occur about an eye-fixed horizontal axis. This provides the observed form of Donders' law, where rotations about the third, eye-fixed torsional axis are minimized. This strategy has different perceptual consequences than Listing's law; for example, it tends to better preserve horizontal lines on the retina (Glenn and Vilis 1992). However, it was initially unclear whether this apparent constraint on Es results from a deliberate control strategy or whether it follows trivially from more fundamental mechanical or neural constraints on Hs and Eh.

Like Es, Hs and Eh each pose a degrees-of-freedom problem for their respective control systems because these segments are mechanically (and behaviorally in some circumstances) capable of rotating in the redundant torsional dimension (Collewijn et al. 1985; Crawford and Vilis 1991, 1995; Hess and Angelaki 1997; Misslisch et al. 1994a). When the orientation vectors of Eh are quantified during a range of human head-free gaze *fixations*, they appear to form (or at least are indistinguishable from) a plane similar to the head-fixed Listing's plane (Radau et al. 1994). The human head also appears to follow Donders' law during head-free visual fixations (Straumann et al. 1991; Tweed and Vilis 1992), but in this case it is more consistent with the Fick gimbal strategy described earlier for Es (Glenn and Vilis 1992; Melis 1996; Theeuwen et al. 1993). This means that all three possible measures (Es, Hs, and Eh) obey Donders' law at least in approximation, but geometrically only two of these rules need to be enforced and the third will simply fall out: but which one is this? Radau et al. (1994) attempted to answer this by quantifying the variance of torsion in each of these segments and found that of the three, static Eh torsion was controlled most tightly and Es torsion was controlled *least* tightly. They concluded that the brain was actually controlling Hs and Eh orientation and that, at least in terms of control, the Fick-like nature of Es orientation was the trivial fall-out of these more fundamental rules. Our first goal was to similarly evaluate the head-free orientation ranges of Es, Hs, and Eh during visual gaze fixations in monkeys.

Knowing the orientations of the eye and head during gaze fixations does not tell us how these segments rotate to achieve these positions. Because of the noncommutativity of rotations, Donders' law can never be achieved by consistently rotating a given segment about the shortest path axis orthogonal to current and desired pointing direction. With Listing's law, there is a kinematic rule that selects a single ideal axis of rotation for any one saccade that will preserve eye position in Listing's plane throughout the trajectory (Tweed and Vilis 1990). However, during head-free gaze shifts, this is problematic for both the eye and the head.

First, the eye cannot use a simple kinematic strategy to maintain Listing's law during head free gaze saccades because of the VOR. Each gaze shift typically is accompanied by an initial Eh saccade that is followed by a VOR slow phase, which stabilizes desired eye orientation in space once the visual target is acquired to prevent overshoot while the head continues to move (Bizzi et al. 1971; reviewed in Guitton 1992). The VOR is known to *not* obey Donders' law but rather rotates the eye about the same or nearly the same axis as the head (Crawford and Vilis 1991; Haslwanter et al. 1995; Hess and Angelaki 1997; Misslisch et al. 1994a), resulting in accumulation of Eh torsion (Smith and Crawford 1998). Recent gaze saccade experiments have suggested that the 2-D components of Eh saccades anticipate subsequent VOR slow phases to bring the eye toward a final desired position in the head (Crawford and Guitton 1997b; Tweed et al. 1995). This concurs with the earlier observation that during passive head rotations, saccade-like quick phases drive the eye out of Listing's plane in an anticipatory fashion such that vestibular driven slow phases end up bringing the eye back toward Listing's plane (Collewijn et al. 1985; Crawford and Vilis 1991; Crawford et al. 1989).

Here we consider whether Eh saccades during head-free gaze shifts would similarly drive eye position out of Listing's plane in an anticipatory fashion such that VOR slow phases would end up bringing the eye back into Listing's plane at fixation. This would require very precise control over all the torsional components of the saccade burst generator (Crawford et al. 1997; Henn et al. 1989) during goal-directed gaze shifts. If so, this would be difficult to reconcile with the view that Listing's law emerges from a simple projection of visual vectors onto a saccade command aligned in Listing's plane (Raphan 1997, 1998). Furthermore, this would have important general implications for understanding the organization of eye-head coordination downstream from the common gaze error command (Freedman et al. 1996; Munoz et al. 1992; Robinson and Zee 1981).

Finally, it is not yet clear how the trajectories of head motion subserve the Fick gimbal strategy observed during fixation. In particular, it is not known if Donders' law of the head is maintained during movements or if it is only obeyed between movements. It has been observed that during repetitive back-and-forth head movements, humans transiently violate the Fick gimbal strategy in favor of a ''minimum rotation'' strategy, where the head simply rotates about the axis orthogonal to the plane of its initial and final facing directions (Tweed and Vilis 1992). However, it is not yet clear what happens during normal, nonrepetitive movements. Presumably the head-control system might achieve purely vertical or horizontal rotations about constant axes very similar to those seen in the telescope-like physical implementation of a Fick gimbal. In other words, it might maintain Donders' law *throughout* the course of each movement by rotating the head about a constant, *space*-fixed vertical axis during horizontal movements and a constant *head*-fixed horizontal axis during vertical movements. If so, then the head would behave both statically and dynamically like Fick gimbals.

However, by corollary, because these horizontal and vertical axes of Fick coordinates are fixed thus in different segments, in some situations mechanically rigged Fick gimbals must rotate the controlled object about *nonconstant* axes, i.e., axes that do not have a constant orientation in space. In particular, during large oblique head movements, the head-fixed horizontal axis would have to rotate along with the head around the space-

fixed vertical axis during the movement to maintain head orientation at zero torsion in Fick coordinates. In other words, a mechanically rigged Fick gimbal with torsion fixed at zero rotates about nonconstant, torsionally looping axes during oblique movements. Alternatively, without this dynamic constraint, any final Fick orientation can be reached from any initial Fick orientation by a *constant* axis of rotation that transiently *violates* the Fick form of Donders' law during the movement. It is currently unknown if the head-control system optimizes head axes in this fashion during oblique head movements or maintains Donders' law *during* movements according to the previous alternative.

The latter question is important, because it may reveal whether the Fick gimbal strategy of the head is mechanical or neural in origin, and if neural, whether it is implemented in a feed-forward fashion while planning the movement or within an internal feedback loop during the movement. Moreover, if this strategy is neural in origin, then it might show some capacity for plasticity or task-dependence (Tweed 1997), which could in turn reveal the normal functional significance of the Fick gimbal strategy of the head. For example, even if the Fick strategy is neural in origin, it still may function to optimize either anatomic (Radau et al. 1994; Theeuwen et al. 1993), perceptual (Glenn and Vilis 1992), or task-related requirements. We set about to test among these options both in normal gaze shifts and also in a pin-hole goggle paradigm where several task constraints (that might normally encourage or enforce the Fick strategy) were removed (Crawford and Guitton 1997b). Some of these experiments have been described briefly in abstract form (Crawford and Guitton 1995; Guitton and Crawford 1994; Klier et al. 1998).

METHODS

Surgery and equipment

Three monkeys (*Macaca fascicularis*), henceforth designated *animals M1*, *M2*, and *M3*, underwent aseptic surgery under general anesthesia (isoflurane, 0.8–1.2%) during which they were fitted with an acrylic skull-cap. Two 5-mm-diam scleral search coils also were implanted in the right eye of each animal for 3-D recordings, using a method described previously (Crawford and Vilis 1991; Tweed et al. 1990). Animals were given analgesic medication and prophylactic antibiotic treatment during the postsurgical period. Experiments commenced after 2 wk of postoperative care. All animal care and experimental procedures were approved by the McGill and/or York Animal Care Committees and were in accordance with the Canadian Council on Animal Care policy on the use of laboratory animals.

Before experimentation, animals were placed in a Crist Instruments primate chair, with the top plate modified to reduce encumbrances to head movement. Specifically, for the first two animals (*M1* and *M2*), the top plate was integrated to fit flanges on custom-made plastic monkey collars, such that the collar slid in, leaving a 1-cm-thick, 7.5-cm-diam ring of rigid plastic around the neck (Crawford and Guitton 1997b). A recessed hollow also was built into the front of this plate so that it did not interfere with the animal's chin on looking down. Other than gaze directions $>50°$ downward (which we did not explore), rotational head movements and the visual range were left unobstructed by this apparatus. However, the rigid structure of the materials surrounding the neck restricted translational movements of the head and forced the animal to sit upright without slouching. To test whether these mechanical constraints might interact or interfere with the neural constraints on head orientation, a different chair was used with the third animal (*M3*). In the latter chair, the rigid structures surrounding the neck were replaced altogether by a reenforced cloth that was buckled snugly at the animals back during experiments, similar to the system used by Freedman and Sparks (1997). This arrangement allowed *animal M3* to obtain its accustomed slouching posture and make unobstructed head translations over a reasonably wide range.

During experiments, the primate chair was placed such that the head was at the center of three mutually orthogonal magnetic fields (1.5 m diam, giving uniform quaternion measurements within ± 15 cm of center). Signals were low-pass filtered at 125 Hz, 12 dB/octave and digitized at 100 Hz from the eye coils and from two orthogonal 1-cm ''head'' coils embedded in plastic. For head-free experiments, the head coils and wire leads for the eye coils were secured with nylon screws to the skull-cap. These preparatory procedures were performed with the head fixed via a bolt screwed to a frontally placed cylindrical implant, which could be detached using a quick release mechanism, and the head-restraint assembly swung backward on the primate chair for relatively unencumbered head-free recordings. Because chest orientation was not measured, head orientation relative to the chest could not be precisely computed. However, given that the chest was nearly stationary during experiments, our measures of Es and Hs were roughly equivalent to eye and head relative to the chest. Some translational movement was observed qualitatively during experiments with *M3* but was not quantified. Therefore this study could not directly address the stability of rotational axes in translational space (Melis 1996) or the contributions of head translations to gaze control but rather focused on measurements of behavioral constraints on 3-D orientation.

Visual tasks and training

All training was performed with the head unrestrained. Animals initially were trained to sit upright and face forward in the primate chair. Animals were next trained to fixate ''primate treats'' held at a 80 to 100 cm distance throughout a large range of the visual field (Crawford and Guitton 1997b). These targets were held at the end of forceps and moved very rapidly from location to location to avoid pursuit movements. If the animal faithfully followed the visual target, it (the treat) was fed manually to the animal. This procedure was continued until the animal would follow the target with discrete gaze saccades for ~3 min before acquiring the reward. Other than this requirement, no time constraints were added, i.e., animals were always allowed make self-paced gaze shifts between targets using an eye-head coordination strategy of their own choosing. This paradigm, where the visual target was the reward, was designed to emulate a biologically natural pattern of motivated gaze shifts. It resembled the food/barrier paradigm used extensively to investigate head-free gaze shifts in the cat (e.g., Guitton et al. 1990) except that a rich amount of visual motion information was available during repositioning of the target.

During control experiments, four standard paradigms were used. First, the radial task: animals oriented toward the target with gaze saccades toward and away from center, following a roughly even distribution of directions. A reproducible center point was maintained by fixing a pair of nylon strings orthogonally across the front of the Helmholtz coils forming a cross-hair directly ahead of the right eye in magnetic field coordinates. Among other things, this task was used to determine a reference point with a behaviorally natural combination of eye and head positions (see following text). Second, the repetitive task: using visual aids that could be repositioned at the front of the Helmholtz coils as a guide, targets were repositioned back and forth to induce repetitive horizontal/vertical gaze shifts at various vertical/horizontal levels. Third, the hour-glass paradigm (illustrated graphically in RESULTS): similar to the last, but inducing horizontal, vertical, and oblique movements in a reproducible but nonrepetitive fashion. Finally, the random task: the target was repositioned throughout the visual range in a nonrepetitive 200-s sequence that covered the range

in as random an order as possible. Targets were held as eccentrically as possible without inducing whole body rotations (as determined through trial and error): approximately ±60–80°. These measurements were repeated on subsequent days for a total of 10 control experiments in animal *M1* and 19 in *M2*. Nine further random-task experiments were obtained in *animal M3*, but this last animal could not be induced to comply with the task requirements of the more demanding paradigms.

When initial training was completed and control data were gathered, animals also were fitted with a pair of opaque plastic goggles that attached (via wing nuts) to screws implanted in the skull-cap. These goggles were shaped to the contour of the monkeys' faces with additional soft flanges at the edge so as to completely occlude vision in both eyes. A single round aperture then was added such that the right eye was given a useful visual range of ±4°. Details of this procedure have been described elsewhere (Crawford and Guitton 1997b). Forty-five minute per day training sessions with the goggles then commenced. Initially, animals were trained to visually follow slow movements, and then as the speed of their gaze movements increased, targets were displaced rapidly over a wide range until they easily made rapid searching head movements to visually acquire the target. Invariably animals mastered horizontal gaze shifts first, then vertical gaze shifts, and finally oblique gaze shifts. Between training periods, the goggles were removed, and the animals were returned to their normal housing area. As judged subjectively, the total training time required for rapid, accurate, and discrete movements in all directions and throughout the entire range required ~4 wk in *animal M1*, and ~10 days in *animal M2*. After this training period, the radial and random tasks were repeated both without and then with the goggles, for a total of five experiments in *animal M1* and 9 in *M2*. (Further behavioral experiments done with these animals/preparations were reported elsewhere) (Crawford and Guitton 1997b.)

Data analysis

The analysis of 3-D movements evokes several challenging computational problems, such as nontrivial coordinate system problems, degrees-of-freedom problems, and the noncommutativity of rotations (Haslwanter 1995; Tweed 1997). Thus a very rigorous and clearly defined quantification of the data was required. A computer was used to convert coil signals into eye position quaternions using a method described previously (Tweed et al. 1990). Quaternions were used because, unlike raw coil signals, they provide an accurate and convenient measure of 3-D eye position over a 360° range. Quaternions represent each eye position as a fixed-axis rotation from some specified reference position (Westheimer 1957). Quaternions are composed of a scalar part q_0, and a vector part **q.** It is the vector part that is used for representation of data. To interpret the data, one need only understand that **q** is parallel with the axis of eye rotation, and its length is proportional to the magnitude of this rotation. To be specific, a quaternion is related to the axis and magnitude of a rotation as follows

$$q_0 = \cos(\alpha/2) \quad (1)$$

$$\mathbf{q} = \mathbf{n} \sin(\alpha/2) \quad (2)$$

The angle α is the magnitude of the rotation and **n** is a 3-D unit vector parallel to the axis of rotation. At reference position α = zero and so $q_0 = 1.0$ and **q** = zero. The quaternion vector can be broken down into three components, ordered such that q_1 represents torsional position, q_2 represents vertical position, and q_3 represents horizontal position, with signs arranged to satisfy the right-hand rule. Throughout this paper, the Hs and Es quaternions are expressed in a right-handed coordinate system aligned with the space-fixed magnetic fields of the Helmholtz coils.

The choice of reference positions for the eye and head is potentially somewhat arbitrary in the head-free preparation because an infinite number of eye-head combinations could subserve a single gaze direction, and there may not be a rigorously definable ''primary position'' for Es (Glenn and Vilis 1992). To choose a convenient and behaviorally meaningful set of reference positions for each experiment, we scrutinized the spread of eye and head coil signals during fixation of the central target in the head-free radial task and then selected a point where both the 2-D pointing directions of the eye and head were near the center of their somewhat variable ranges (see Fig. 2). This resulted in a reference position for Es orientation defined in magnetic field coordinates, where gaze was directed straight ahead along the forward pointing field; a behaviorally central reference orientation for Hs orientation defined similarly in field coordinates; and a behaviorally central reference orientation for Eh, defined in head coordinates, which were themselves defined by the intersection of the magnetic fields with the head when it was at its reference position.

The position of Eh then had to be computed from both the eye coil signals (which directly gave eye position in space) and the head coil signals. In one dimension, this would be done by subtracting head position from gaze position. In three dimension, this was done by dividing the Es quaternion by the Hs quaternion (Glenn and Vilis 1992) as follows

$$Eh = Es(Hs)^{-1} \quad (3)$$

This provides the quaternion for eye position in head coordinates. As described in the preceding text, the alignment of these coordinates with the head was initially quasiarbitrary, i.e., depending on the alignment of the magnetic fields with the head when it was at the chosen reference position. However, in some cases, these data were rotated into a new coordinate system such that the head-free analogue of Listing's plane aligned with the new coordinates, and the Eh data were measured relative to a new reference position analogous to primary position (Tweed et al. 1990). On occasion (e.g., Fig. 5) a similar procedure also was used with Hs quaternions.

2-D ''pointing vectors'' were computed from quaternions as described previously (Tweed et al. 1990). These unit vectors typically were projected onto the frontal plane to indicate where the eye or head was pointing. For the eye, these vectors align with the visual axis in either space coordinates, i.e., gaze, or head coordinates. For the head, they can be thought of as the aiming direction of the nose. Finally, instantaneous angular velocity vectors were computed from position quaternions using the method described previously (Crawford and Vilis 1991). These were vectors aligned with the instantaneous axis of rotation of length equal to the instantaneous angular speed of rotation. Like the quaternion vectors, the angular velocity vectors were expressed according to the right-hand rule, as described further in the following text. Because translations could not be measured, ''axis constancy'' in the RESULTS refers to the *orientation* of the velocity vector during movements.

To quantify the orientation ranges of Es, Hs, and Eh, first-, second-, and third-order fits were made to Es, Hs, and Eh quaternions using the previously described procedure (Glenn and Vilis 1992; Radau et al. 1994; Tweed et al. 1990). The following formula provides the equation for a second-order fit for a generic position quaternion (q)

$$q_1 = a_1 + a_2q_2 + a_3q_3 + a_4(q_2)^2 + 2a_5q_2q_3 + a_6(q_3)^2 \quad (4)$$

This is the 3-D analogue to the equation for a 1-D line in 2-D space and represents a description of torsional position as a function (through parameters a_1–a_6) of various combinations of vertical and horizontal position up to the squared terms. A first-order fit uses only the first three terms, whereas a third-order fit adds four more terms (a_7–a_{10}) for the cubic combinations of q_2 and q_3. Once such a 2-D ''surface'' of best fit had been computed, the standard deviation of the torsional components of all actual positions from this fit was computed using the method described previously (Tweed et al. 1990).

An additional measure of the 3-D range, called the ''gimbal score'' also was applied to the head-orientation data (Glenn and Vilis 1992).

For this test, the head quaternion data first were rotated into alignment with the pitch-yaw axes plane using the parameters derived from *Eq. 5* and then fit to the following equation to provide the single term *s*

$$q_1 = s(q_2 q_3 / q_0) \quad (5)$$

The resulting number provided a convenient measure of the data's fit to a zero-torsion range at some point along the continuum from Fick coordinates to Listing coordinates to Helmholtz coordinates (described further in RESULTS).

The preceding measures of fit and variance were applied to several subranges of the data selected on the basis of various velocity criteria. For example, the ''fixation'' range was defined to be those positions where the velocity (more correctly the 1-D magnitude of 3-D velocity) of both Es and Eh were $<10°$/s. Other, more complex criteria were used to select the position ranges at peak head velocities, at the starts of Eh saccades, at the ends of Eh saccades, at the starts of slow phases, and at the ends of slow phases. Simple but robust algorithms for selection of these subranges (provided in the APPENDIX) were developed on a trial-and-error basis from the recorded 3-D data.

RESULTS

Figure 1 reveals most of the issues and challenges of describing eye- and head-orientation trajectories in 3-D space. These data were selected from a sequence of large, pseudorandom-gaze shifts between widely dispersed peripheral targets (i.e., the random task) in *M1*. The primary object of control, 2-D gaze direction in space, is shown in Fig. 1*A;* — show the trajectories of gaze while it was moving, whereas ◆ indicate points of fixation between these movements (where both the eye and head were stationary). Note that these data portray gaze as the tip of a unit vector, projected onto the page as if from behind the subject (the perspective is indicated by the head caricatures in the figures). When similar representations are used below, they will be referred to as ''gaze vectors'' (for Es) or ''direction vectors'' (for Hs). This particular set of data (Fig. 1) was selected to show a sequence of very large pseudorandom gaze shifts between eccentric targets, roughly corresponding to the limit of the obtainable range in our preparation. Clearly, the animal could acquire a large range of visual targets in all directions (with the downward visual range somewhat limited because it was obscured by the primate chair).

The remainder of Fig. 1 (*B–E*) uses a different convention to portray 3-D *orientations* from the same subset of data as Fig. 1*A.* Again, both 3-D trajectories during movements (—) and orientations during eye/head fixations (◇) are shown. However, these data now represent 3-D position vectors. For example, if one chooses any one fixation point or any one point on a trajectory, it is actually the tip of a vector emanating from the origin. Each vector is aligned with the axis of rotation that would take the eye or head from the reference position (defined in METHODS) and is stretched to a length proportionate to the angle of this relative rotation. Furthermore these vectors are oriented according to the right-hand rule, such that a vector pointing upward (thumb of right hand) represents a position rotated to the left (curl of fingers on right hand). Note that these data are portrayed in orthogonal coordinates, where the torsional, horizontal, and vertical coordinate axes are all fixed either in space or in the head. The head caricatures in Fig. 1, *B–E,* indicate that these coordinates and 3-D position vectors are viewed from the right of the subject throughout the figure, such that they show the horizontal and torsional components of eye and head orientations (head + torso symbols designate space coordinates, whereas head only symbols designate head coordinates).

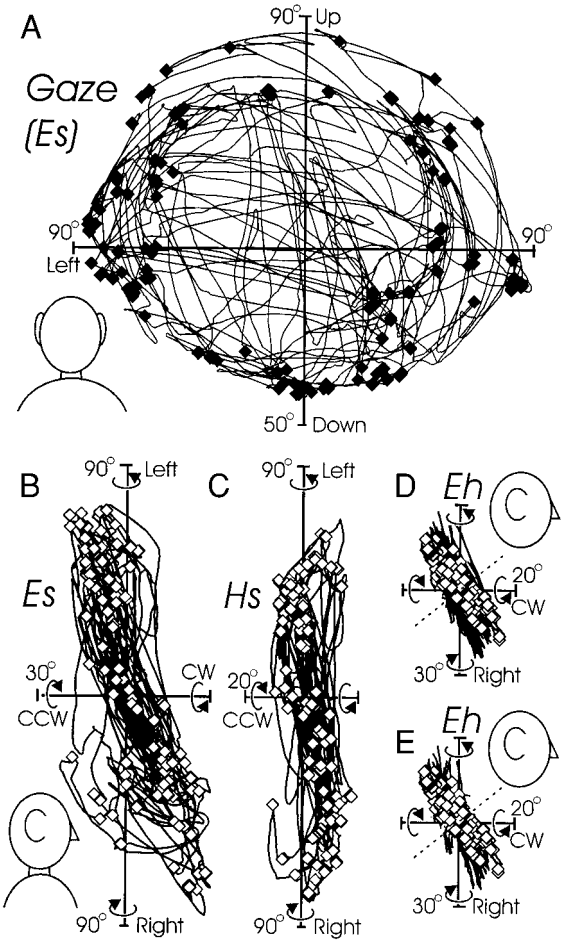

FIG. 1. Basic two- and three-dimensional (2-D and 3-D) kinematics of randomly directed gaze shifts. Same primary data set is used throughout. *A*: projection of 2-D gaze vector tips onto the plane containing the horizontal and vertical magnetic fields. Such a projection results in a nonlinear (~sine of gaze angle) scale that becomes squashed toward the 90° mark. —, gaze trajectories; ◆, fixation points, where both gaze and head velocity are $<10°$/s. Head-and-shoulders symbol indicates that the data are viewed from behind in space coordinates. *B–E*: 3-D kinematics of eye and head orientation, showing ''side'' projections (see head/shoulders) of quaternion vectors. —, orientation trajectories; ◇, fixation data. These plots employ the right-hand rule convention, such that the vertical axis indicates positions rotated horizontally from reference (see curving arrows), and the horizontal axis indicates torsionally rotated positions. *B*: 3-D orientations of the eye-in-space. *C*: 3-D orientations of the head-in-space. *D*: 3-D eye-in-head orientations with trajectories of saccades shown. *E*: eye-in-head orientations with trajectories of slow phases shown. Initial untransformed headcentric coordinates were used in the latter 2 plots, i.e., not Listing's coordinates. *Animal M1* shown.

Figure 1*B* shows the orientations of Es that correspond to the gaze directions in *A.* It is important to remember that in these and all further illustrations, Fick coordinates are not used to represent the data, and thus torsion is *not* rotation about the visual axis. In this case, the torsional coordinate is an axis fixed in space. With these coordinates and data, it is evident that the range of eye torsion in space is relatively compact compared with the horizontal range but still shows considerable variability (~40° peak to peak), both during and between fixations. Thus a flat Listing's plane was not evident in such plots, but at

this point it was not clear whether Es torsion obeyed some other *nonplanar* constraint, was simply much sloppier than head-restrained eye torsion (Tweed et al. 1990), or both.

The remainder of the figure shows the head and Eh orientations that contributed to the Es orientations shown in Fig. 1*B*. Figure 1*C* shows similar vector representations of head orientation in the same space-fixed, orthogonal coordinate system. The head range seems slightly more compressed torsionally and more aligned with the vertical but is otherwise similar to the Es range. However, there is still considerable variability (~30° peak to peak) in torsional head positions during gaze fixations (◇).

Finally, Fig. 1, *D* and *E*, shows orientations ranges of Eh, plotted in the same scale as the preceding data. The fixation points (◇) are the same in both *D* and *E*, showing Eh orientations at the end of multiple-step gaze shifts, where both the eye and head were stationary. However, the position trajectories (underlying continuous lines) have been subdivided to show saccade trajectories (when head was also moving) in *D*, and *VOR slow phase* trajectories in *E*. Compared with the head and Es, which showed considerable variability in torsion both during movement and head/gaze fixation (◇), the Eh fixation range (◇) formed a relatively compact range. This range was clearly most compact along the dimension indicated (- - -). However, the Eh trajectories during movements (—) were less restricted, extending outward from the fixation ranges both during saccades (*D*) and slow phases (*E*).

Although Fig. 1 provides an overview and some clues to the kinematics of eye-head coordination, it also shows the somewhat daunting complexity of deriving simple rules from this complex data. To derive such rules, we had to analyze the data in a more reductive fashion. The subsequent sections will adhere to the following course of analysis, noting first that Es orientation during *fixations* is most directly relevant to vision (the biological task of this system). Second, the head and Eh orientations observed during these fixations thus presumably will be the goals of the eye- and head-control systems. Therefore we will begin by considering the ranges of Es orientation during stable gaze fixations, and the ranges of head and Eh orientation that contribute to these positions (◇ in Fig. 1). After establishing the rules that govern these ranges, we then will consider the movement trajectories used to obtain these ranges.

3-D fixation ranges of Es, Hs, and Eh

Figure 2 introduces the subject by showing the ranges used to fixate a single target. These data were selected from a series of gaze fixations toward a central, straight-ahead target, reached by a radial pattern of centripetal gaze shifts (not shown) from a wide distribution of peripheral targets (the radial task). Figure 2, *top* (*A–C*), shows the horizontal and vertical components of 2-D direction vectors. The gaze vectors for Es (*A*) form a tight group around the zero point, showing that the target was foveated accurately after each centripetal gaze shift. In contrast, the vertical and horizontal components of the head (*B*) and the Eh (*C*) vectors show considerable variability during the same fixations. This is possible because an infinite number of combinations of head (*B*) and eye (*C*) position can give rise to the same gaze direction in space (*A*). Considering only gaze fixations within ±1° of the central fixation point, the range of horizontal head position (quantified

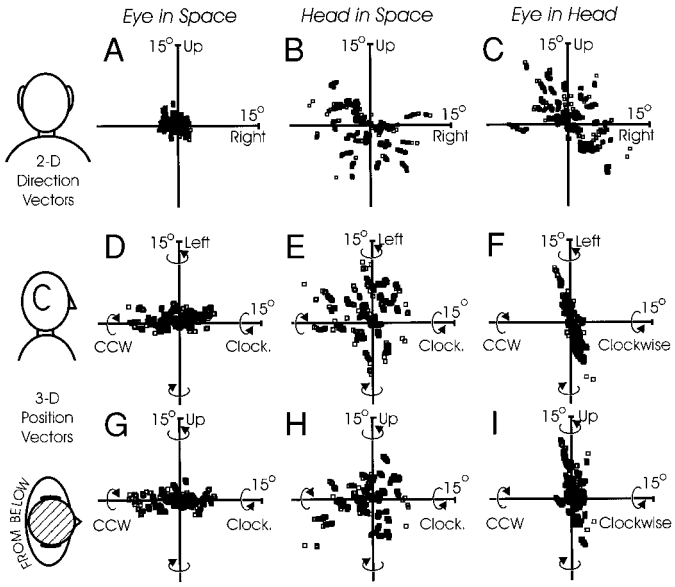

FIG. 2. Two- and 3-D distributions of gaze, eye, and head position during steady fixation of a central target. Data were selected from the radial task, where the animal arrived at the central target (*A*) from gaze directions in a variety of eccentric, uniformly distributed directions (trajectories not shown). *Top, A–C*: frontal projections of 2-D pointing vectors for gaze direction (*A*), head direction (*B*), and eye-in-head direction (C*). Middle* and *bottom, D–I*: projections of 3-D orientation vectors for eye in space, head in space, and eye in head, using the right-handed rule. *Middle*: horizontal position as a function of torsion (i.e., a ''right-sided'' perspective), whereas *bottom* plots vertical position as a function of torsion (requiring a slightly unorthodox perspective of the rotation axes from below the head/body to have upward positions upward and counterclockwise positions rightward on the page). *Animal M1.*

as 4 SD, i.e., ~98% of the data) was 14.5° in *animal M1* and 10.0° in *M2*, averaged across all radial task experiments. The average vertical head range was also 14.5° in *animal M1* but lower at 5.2° in *M2*. (Note that, as follows trivially, Eh showed almost identical variations). Such 2-D variations have been described before (e.g., Freedman and Sparks 1997; Radau et al. 1994) and will not be examined further here. The point to be taken is that from this 2-D perspective, the system appeared to control gaze direction much more tightly than the precise combinations of eye and head position that contributed to gaze.

The 3-D orientations of the same eye and head data revealed a somewhat different picture. The remainder of Fig. 2 shows the torsional orientations of the eye and head plotted against horizontal position (*middle*) and vertical position (*bottom*). In the case of Es (*left*), the torsional orientation is considerably more variable than either horizontal (*D*) or vertical (*G*) position. In this particular task, the space-fixed torsional coordinate happens to align with the visual axis. Most interestingly, whereas horizontal and vertical position were controlled tightly to land gaze on target (*A*), the torsional orientation of Es *around* the line of gaze varied by ≤20° for this same single target direction (Fig. 2, *D* and *G*). Using the 4 SD definition from the preceding paragraph, the average torsional range of Es was 9.3° in *animal M1* and 13.7° in *M2*, considerably larger than the ±1° gaze window used to compute these values. (*Animal M3* refused to fixate the central target over enough repetitions to perform this measurement but showed qualitatively similar results).

In contrast, Eh torsion formed a very compact range much smaller than the horizontal (*F*) or vertical (*I*) range of Eh

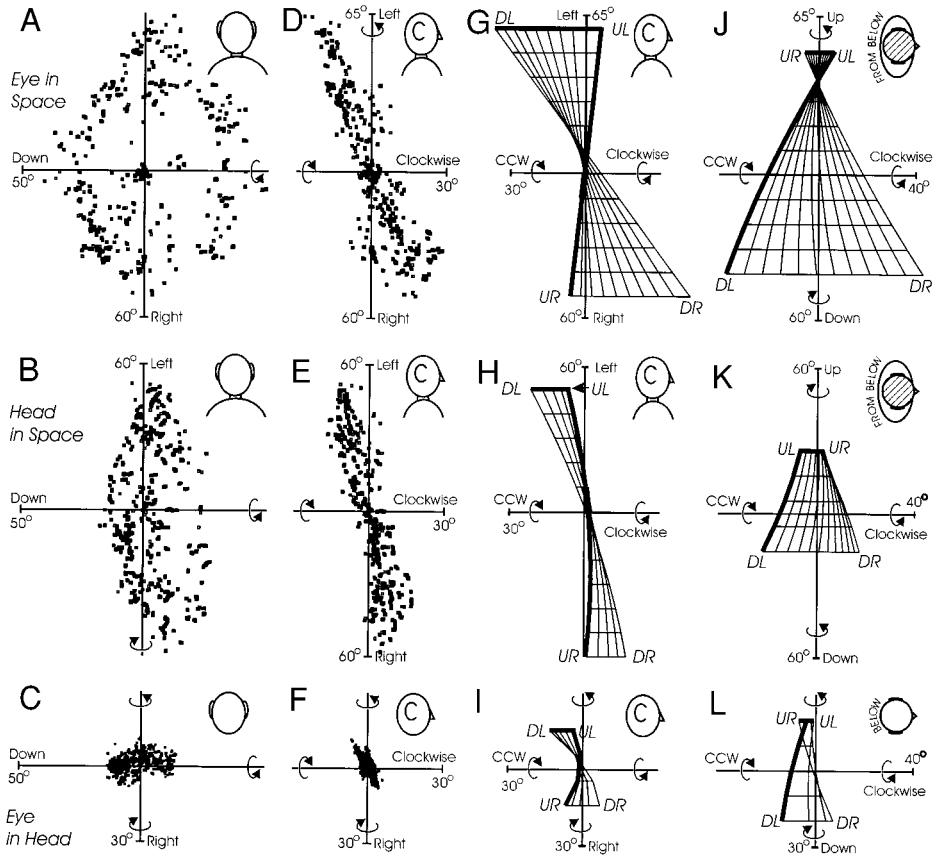

FIG. 3. Fixation ranges of eye in space (*top*), head in space (*middle*). and eye in head (*bottom*) during random-gaze shifts. *A–F*: quaternion vectors are plotted according to the right-hand rule from the behind perspective (*A–C*) and side perspective (*D–F*), as indicated by the caricatures. Eye-in-head data have not been rotated into Listing's coordinates. Same data set is used throughout. *G–L*: 2nd-order surface fits to the fixation data in previous columns. Each grid indicates 10° vertical/horizontal across the rectangular surface as it would be seen from a ''behind view'' (not shown), with limits corresponding approximately to the range of data used in the fit. (Because the 2-D data ranges are somewhat rounded or oval shaped, whereas the illustrated fits are square, they overextend the data range at the corners.) Thickened lines correspond to the upper and leftward (in terms of gaze direction) edges of the illustrated fit, and the corners of the fit are labeled (DL, down-left; UL, up-left; UR, up-left; DR, down-right) according to gaze direction. *G–I*: side perspective, corresponding directly to *D–F*. *J–L*: below perspective of the same data, showing the dependence of torsion on vertical position. *Animal M1*.

positions used for this one target. Indeed, even for a single target these ranges give the appearance of a tilted Listing's plane, suggesting that eye orientation was only allowed to vary within a quasiplanar range. Because torsional variance previously has been quantified using the single standard deviation (e.g., Glenn and Vilis 1992; Radau et al. 1994), we henceforth will follow the same convention. The average (across experiments) torsional SD of Eh was only 0.99° in *M1* and 0.72° in *M2* in this task (where gaze was within ±1° of center), considerably less than those of Es (2.32 and 3.43°, respectively). The distribution of head orientations (Fig. 2, *E* and *H*) was intermediate between these extremes, showing roughly equal ranges of torsion, vertical, and horizontal variance (2.99, 2.46, and 3.07° SD, respectively; averaged across experiments and then between animals).

Thus from this data, it would appear that the 2-D contributions of the eye and head to gaze direction were controlled rather loosely compared with gaze in space (*top*) but that Eh torsion was controlled much more tightly than Es torsion (*middle* and *bottom*). However, the rule governing head position is not yet clear from Fig. 2. To more completely characterize these rules, we next examined orientations over a much wider distribution of gaze fixations toward multiple target directions.

The *first two columns* of Fig. 3 show 3-D orientation vectors during fixations toward a wide range of target directions, as best seen in *A.* (The data range in the previous Fig. 2 corresponds roughly to a small subset of the data near the coordinate origins in Fig. 3.) In Fig. 3, Es (*top*), Hs (*middle*), and Eh (*bottom*) orientations are viewed from the behind perspective (*1st column*), i.e., vertical versus horizontal, and side perspective (*2nd* column), i.e., torsion versus horizontal. From the behind perspective, it is evident that the Hs fixation range (*B*) was elongated in the horizontal dimension, whereas the Eh range (*C*) was elongated in the vertical dimension. Because the Es range (*A*) roughly corresponds to the sum of the latter two ranges, the head thus contributed relatively more to the horizontal Es fixation range, whereas Eh contributed relatively more to the vertical Es range. This was typical in our animals and matched previous reports of head-free primate behavior (Freedman and Sparks 1997; Glenn and Vilis 1992) but was not further quantified. From the side perspective, it is evident that for a large range of fixation directions, torsional Es (*D*), Hs (*E*), and Eh (*F*) ranges were somewhat restricted, but the precise nature of this restriction remains incomplete in these plots.

To reveal the 3-D shape of these flattened position ranges, we employed the same methods used in similar human studies (Glenn and Vilis 1992; Melis 1996; Radau et al. 1994), applying second order ''surface'' fits (*Eq. 5*). The remaining *rightward columns* of Fig. 3 graphically depict the surfaces fit to the data shown in the *first two leftward columns.* These plots show the dependence of torsional position on the other components of position, where each grid mark indicates 10° of horizontal/vertical excursion. The *third column* of Fig. 3 shows the side view corresponding to the *second column,* whereas the *rightmost column* of Fig. 3 depicts the ''below'' view, showing the dependence of torsional orientations on vertical positions in a way that orients upward position upward on the page. (Imagine that the plots in the *3rd column* were rotated 90° about the torsional axis, bringing their bottom parts out of the page, to obtain the ''below'' perspective in the *4th row*). The rectan-

gular corners of these fits, which usually extended beyond the more rounded range of the actual data, are labeled according to the corresponding 2-D pointing directions (DL, UL, UR, DR) to facilitate interpretation.

The fits to the Es and Hs data show the same striking feature: the ranges are twisted into a flattened 2-D bow-tie-like shape. This is most evident from the side views (note that the apparently greater ''fanning out'' of the Es bow-tie compared with the head bow-tie is largely due to the wider distribution of vertical gaze positions rather than a greater twist to the bow-tie). The same bow-tie like twist is evident in the below views of this data as well (*right column*), but the vertex of the twist was shifted upward on the graph (i.e., toward an upward position). The latter is simply a perspective effect: because the bow tie is tilted backward (i.e., upward about the horizontal axis) from the side perspective, its vertex automatically looks shifted from the ''below'' view. In concrete terms, this bow-tie shape signifies that Es/Hs assumes *relatively* (compared with its neighboring corner on the illustrated plot) counterclockwise orientations in down-left (DL) and up-right (UR) positions and assumes relatively clockwise orientations in up-left (UL) and down-right (DR) positions. (Note that this description is only meaningful in the current orthogonal, space-fixed coordinate system).

To be consistent, we also have plotted the second-order surfaces fit to the Eh data (*bottom*). These also show a similar bow-tie twist in this particular example but were highly variable. For example, the ''twist score'' (described in more detail in the following text) of the Eh range across experiments was 3.3 times as variable as the Es twist score [quantified as the average ratio of the standard deviations of parameter a_5 (*Eq. 5*) across all random-task experiments, further averaged across all 3 animals]. This variability may have been exaggerated because the Eh ranges were too small (Fig. 3*E*) for this method to provide a highly meaningful fit (as pointed out by Radau et al. 1994). Therefore we did not further investigate the subtleties of the shape of the Eh fixation range but rather focused on its torsional ''thickness.''

Quantifying the torsional thickness of the fixation ranges

In quantifying the 3-D ranges of eye and head orientation in humans, two measures have proven useful: the parameters used to form the fits illustrated in Fig. 3, and the standard deviation of torsional eye position (in the actual data) from these ideal 2-D fits (Glenn and Vilis 1992; Radau et al. 1994). We employed the same approach to quantitatively address two questions: which of the three segments (Es, Hs, and Eh) are constrained most tightly by Donders' law, and what form does this law take in each of these segments?

Figure 4 shows torsional standard deviations from first-, second-, and third-order fits to all three segments, computed from random-task fixation data such as those illustrated in Fig. 3. Data from all three animals are plotted separately in *A–C*, whereas each bar represents a value averaged across all random-task measurements in one particular animal. In each case, the bars are grouped according to the order of the fit used to compute the relative torsional standard deviation. The first point to be taken from this figure is that as the order of the fit increased, the torsional variance from this fit decreased. For example, note how the average torsional SD

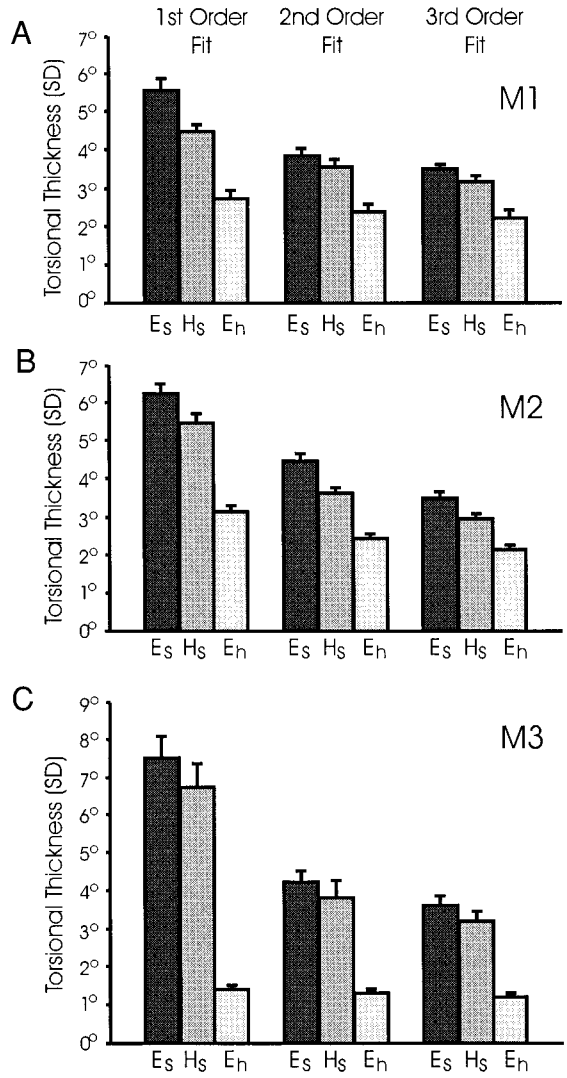

FIG. 4. Quantitative comparison between torsional thickness of eye-in-space (Es), head-in-space (Hs), and eye-in-head (Eh) fixation ranges at each order of fit. Major bars show mean values of torsional standard deviations (from 1st-, 2nd-, and 3rd-order surface fits) averaged across all random task experiments, and error bars provide SEs across experiments. *A*: *animal M1*. *B*: *animal M2. C*: *animal M3.*

for Es (■) dropped dramatically between the first- and second-order fits and dropped further at the third-order fit. However, note (in Fig. 4) that the jump from first- to second-order fits produced the greatest effect in Es and Hs variance (compared with the 2nd–3rd interval), whereas the torsional SD of Eh showed a steady, less dramatic decline toward higher orders of fit (perhaps due to the problems in fitting the head-free Eh range mentioned earlier). Nevertheless, statistically significant ($P < 0.001$) decreases in variance occurred across both intervals (i.e., 1st–2nd and 2nd–3rd) for each and every case for Es, Hs, and Eh, in all three animals. In summary, although each increase in the order of fit decreased the torsional variance of Es, Hs, and Eh in the statistical sense, visual inspection of the data (Fig. 4, see particularly *animal M3*) suggested that the jump from first to second order gave the most important improvement in the Es and Hs fits, whereas second- and third-order terms appeared to have little effect on the Eh fit.

The second point to be gleaned from Fig. 4 is that there were consistent differences between the torsional variance of Es, Hs, and Es, regardless of which order of fit was used. First, the torsional SD of the Es range was always greater than the torsional variance of the Hs range. This was true in all animals, no matter how complex were the parameters of the fit (1st, 2nd, or 3rd order). In each and every individual case, this difference was statistically significant (range of $P \leq 0.0005$–0.007 in *M1* and *M2*, $P \leq 0.04$ in *M3*). Similarly, in each and every case in all animals, for all levels of fit, the torsional SD of the Hs range was significantly larger than the torsional SD of the Eh range ($P \leq 0.0005$). Thus even at a third-order fit the torsional SD of Es (mean across animals: 3.55°) was greater than the torsional variance of Hs (mean 3.10°), which in turn was greater than that of Eh (mean 1.87°). This relative ranking agrees with the qualitative descriptions provided above (Figs. 1–3), as well as observations in humans (Radau et al. 1994). According to the arguments employed by Radau et al. (1994), this suggests that Donders' law was only *enforced* by the individual control systems of Hs and Eh, whereas the Donders' law for Es was simply a geometric byproduct of the other two laws.

From the preceding, data we draw three interim conclusions necessary for the further development of our analysis: first, the motor implementation of Donders' law in Es during head-free gaze *fixations* can be attributed to *relatively* tight 3-D control of Hs and Eh. Second, the rule governing head orientation during fixation gives rise to a decidedly nonplanar, twisted range. Third, Eh orientation vectors were restricted to a relatively thin quasiplanar (or indeterminately twisted) range. These observations are in close agreement with the human data (Glenn and Vilis 1992; Radau et al. 1994). On the basis of these observations, we then analyzed the segmental *trajectories* that give rise to these fixation constraints.

3-D eye-in-head trajectories

On the basis of head-fixed data (Ferman et al. 1987b; Straumann et al. 1995; Tweed and Vilis 1990; Tweed et al. 1994), it might seem reasonable to hypothesize that Eh would obey Donders' law (i.e., remain in Listing's plane) at all times throughout a head-free gaze shift, with only minor and pseudorandom ''torsional transients.'' However, this hypothesis is problematic because head-free gaze shifts include substantial periods where gaze is stabilized by VOR slow phases. Slow phases are known to violate Listing's law in that they tend to rotate the eye about almost the same axis as the head (Crawford and Vilis 1991; Misslisch et al. 1994a). Thus if the head rotation axis does not align with Listing's plane, a slow phase will tend to drive eye torsion out of Listing's plane. Moreover, even if the head axis does align with Listing's plane, the complex kinematics of eye rotation will cause the eye to deviate torsionally as a function of eye position (Crawford and Vilis 1991). How does the head-free gaze control system deal with this problem?

Figure 5 provides several clues to the solution to this problem. Figure 5, *left*, shows the familiar 2-D plot of Eh direction trajectories, where up is up and left is left, etc., whereas Fig. 5, *right*, shows the right-side view of Eh quaternion vectors. The latter have been rotated into a coordinate system that aligns with the first-order fit to the

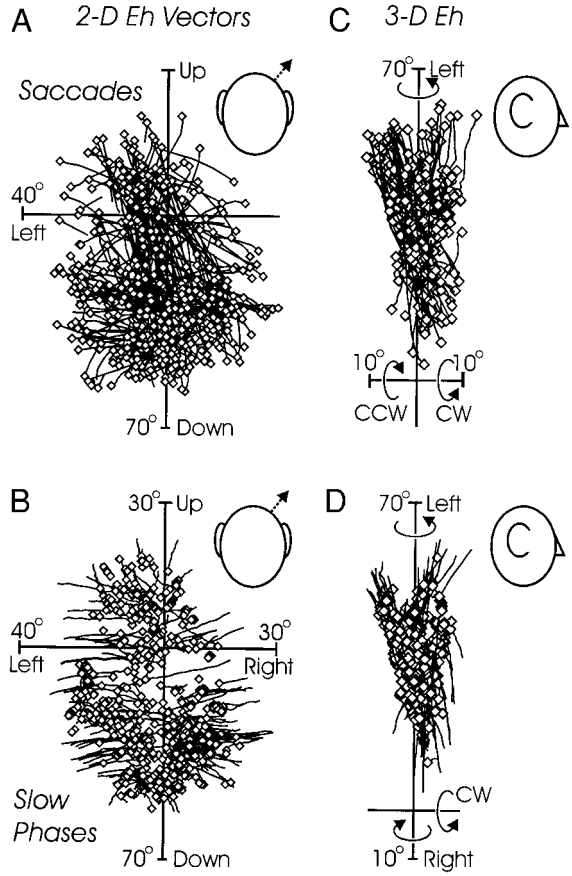

FIG. 5. Two- and 3-D trajectories of saccades and quick phases during head-free gaze shifts. *Top, A* and *C*: saccades, where —, trajectories; ◇, saccade endpoints. *Bottom, B* and *D*: slow phases, where —, trajectories; ◇, slow phase endpoints. Note that these were mostly multiple-step gaze shifts, as shown in Fig. 6. Therefore some of the slow phases would be the final eye movements preceding stable eye/head fixation, but most would be interim slow phases followed by ≥1 further saccade in the multiple-step gaze shift. *Left*: 2-D gaze projected onto frontal plane in magnetic filed coordinates. Origin is the preferred eye position used to look straight ahead and is not necessarily the center of the mechanical oculomotor range. *Right*: side view of 3-D quaternion vectors, plotted relative to the head-free primary position in Listing's coordinates. *Animal M1*.

associated fixation range. From this data it is evident that the primary position at the origin (where the 2-D Eh direction vector is orthogonal to the fixation range) did not necessarily correspond to the center of the head-free Eh range. Figure 5, *top*, shows Eh saccade trajectories (where ◇ indicate saccade endpoints) during random head-free gaze shifts, whereas *bottom* shows similar 2- and 3-D views of the *slow phase* eye movements from the same data set, and their endpoints (◇). Note that, as shown more explicitly in the next figure, most head movements were associated with several Eh saccades and slow phases. Each and all of these sequential eye movements have been included in Fig. 5.

Focusing first on 2-D direction (Fig. 5, *A* and *B*), it is evident that during the random task, Eh saccades (*A*) were directed in a pseudorandom pattern that tended to land final horizontal and vertical eye position over a roughly homogenous range including relatively eccentric positions (◇). In contrast, slow phases (*B*) tended to center eye position, driving it more exclusively toward less eccentric final positions (◇). This is not surprising, given the known kinematics of head-free gaze control (Bizzi et

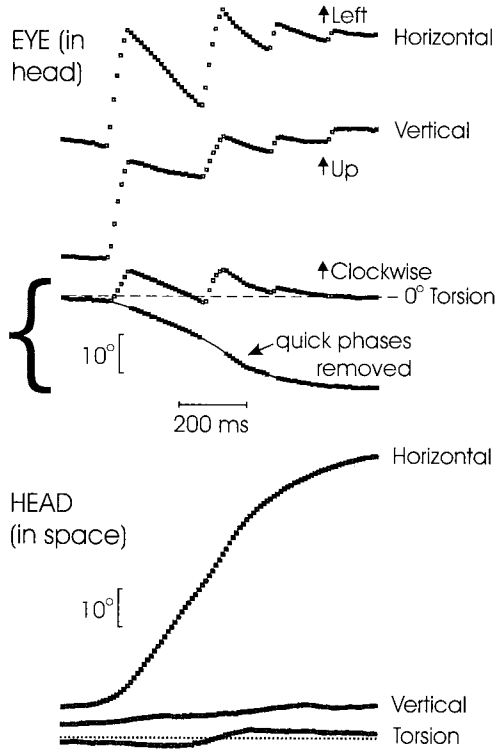

FIG. 6. Temporal kinematics of a typical multisaccade/single head movement gaze shift. *Top*: 3 components of eye position plotted (in headcentric ''Listing's coordinates'') as a function of time. □, saccades; ■, VOR slow phases. Also shown is extrapolated torsional eye position excursion ({) if quick phases are removed, and the remaining slow phase trajectories are fit to a continuous spline curve. - - -, 0 torsion in Listing's plane. *Bottom*: 3 components of head position, plotted in space coordinates but rotated to align with the vertical Fick coordinate. ⋯ , approximates 0 torsion in Fick coordinates. *Animal M1*.

al. 1971). However, how should one expect torsional eye position to behave? From the known kinematics of saccades and the VOR, one might expect the latter to drive the eye out of Listing's plane, whereas each saccade might correct any accumulated deviation from Listing's plane. In fact, the opposite pattern appeared to occur: Eh saccades (*C*) tended to drive final torsional eye position (◇) away from the fixation plane (centered on the vertical axis), whereas VOR slow phases (*D*) tended to land final torsional eye position (◇) closer to the center of the fixation plane. Thus the same rule applied to *all three* dimensions of Eh: saccades tended to drive the eye eccentrically, whereas slow phases tended to center the eye.

The detailed kinematics of this behavior are more clear in Fig. 6, which plots the three components of eye position relative to the head as a function of time during a typical large gaze shift, selected from data recorded during the random paradigm. For reference, the components of head position also are plotted, rotated to align with the vertical axis of the Fick range, such that the horizontal dotted line corresponds approximately to zero torsion in Fick coordinates. As described in the METHODS, the animals were not constrained by time or reward to use any particular strategy to obtain visual targets, and they invariably chose to implement large multiple-step gaze shifts (i.e., with several interim saccades and fixations). This is evident in Fig. 6 where the animal made four consecutively smaller vertical/horizontal Eh saccades (□) during the single head movement, roughly in the same direction as the single smoother head movement profile. Between these saccades, the VOR evidently was engaged, producing slow phases (■) that rotated the eye counter to the head and thus briefly stabilized gaze whenever possible during the gaze shift. Considered from the perspective of 1-or 2-D gaze control, the temporal coordination of this pattern seemed relatively trivial, i.e., saccades shifted gaze toward the target, and then the VOR trivially caused the eye to roll back toward a central position.

From a 3-D perspective, the temporal coordination of this pattern was much more complex. A similar nystagmus-like pattern also occurred in the torsional component of Eh position ({). Note that this Eh data has been rotated into Listing's coordinates, such that - - - represents zero torsion in Listing's plane. The slow phases thus had a considerable torsional component relative to Listing's plane even though the head did not rotate torsionally. As explained in more detail elsewhere (Crawford and Vilis 1991; Smith and Crawford 1998), this accumulation of torsion was primarily a kinematic consequence of rotating the eye about the same axis as the head independent of eye position. In this case, slow phase rotation of Eh in the rightward direction, from an upward eye position, caused torsional eye position to deviate in the counterclockwise direction, as predicted from the laws of rotational kinematics (Smith and Crawford 1998). However, these slow phases did not take the eye away from Listing's plane but rather toward it. This resembled a similar effect described for torsional slow phases during passive head rotation (Crawford and Vilis 1991) except that passively induced slow phases tended to overshoot Listing's plane, whereas these slow phases appeared to land the eye quite accurately within the fixation range (as quantified in the next figure).

The latter effect occurred because each preceding saccade also had a torsional component, but in the opposite direction, such that the overall torsional excursion was negated by the subsequent slow phase. Indeed without such torsional saccades the eye would presumably accumulate a huge Eh torsion, as extrapolated on Fig. 6. Furthermore because the torsional components of these quick phases did not contribute to shifting gaze toward the target and because the torsional direction of the subsequent slow phase could only be predicted by taking both head velocity and eye position into account (Crawford and Vilis 1991), the temporal coordination of this 3-D pattern did not appear to arise accidentally. Instead, it appeared that the system produced specific torsional components in Eh saccades to *anticipate* subsequent vestibular-driven torsional movements, such that ocular torsion always returned to Listing's plane at the end of each slow phase.

To quantify these observations, it was necessary to further subdivide and analyze the Eh position range during multiple-step gaze shifts. Figure 7*A* shows examples of each of these subranges, derived from a single random-task measurement with the use of the algorithms described in the APPENDIX. The 3-D data are viewed from the side (i.e., torsional position vs. horizontal position) in coordinates rotated to align with the head-free Eh fixation range. The first example (Fig. 7*A*, *left*) shows the latter fixation range explicitly, revealing a torsionally compact group of Eh positions. The remaining examples show Eh positions at various start/endpoints of the saccades and slow phases from the same data set. The rest of Fig. 7 (*B–D*) shows the SDs of torsion from each of these ranges, relative to a second-order fit made to the fixation range at gaze

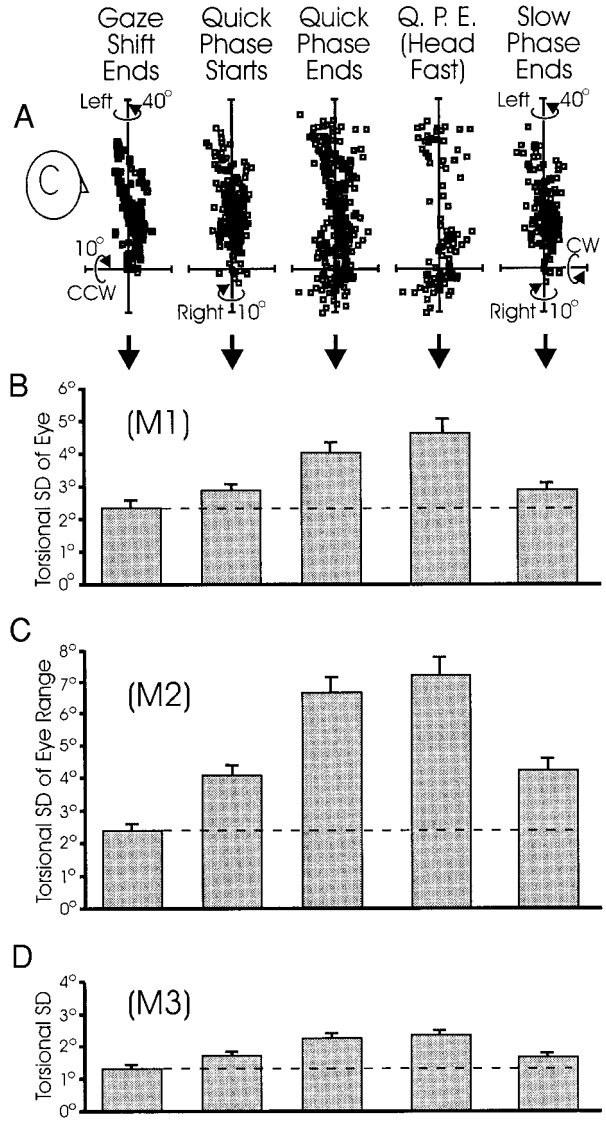

FIG. 7. Quantitative torsional eye-in-head ranges during different stages of the gaze shift. *A*: examples of 3-D eye-in-head position ranges during (1) fixation at gaze shift ends, (2) the starting positions of quick phases throughout gaze shift, (3) the endpoints of all quick phases, (4) the endpoints of quick phases where head velocity >150°/s, and (5) the endpoints of all slow phases during gaze shifts. Positions selected automatically according to the velocity criteria described in text from one random-gaze shift sequence (*animal M1*) and plotted in head-free Listing's coordinates fit the fixation data. *B*: torsional standard deviations of the same 5 position ranges (aligned as already mentioned), as compared with 2nd-order fit to the fixation data for each experiment. Data are averaged across all random task experiments in *animal M1*, with error bars showing SEs across experiments. *C*: same as *B* but computed for *animal M2*. *D*: *animal M3*.

shift ends. The individual bars show average values across all head-free random paradigm measurements (with error bars showing SEs across measurements) in *animals M1* (*B*), *M2* (*C*), and *M3* (*D*). These bars have been aligned in vertical columns with the example ranges in Fig. 7*A*, to facilitate comparison between these columns, where the fixation data (*column 1*) establishes the baseline (– – –) for such comparisons.

Figure 7, *second column*, shows eye positions at the *initial* points of Eh saccades (labeled as quick phases) sampled throughout the multiple-step gaze shift. Compared with the baseline, this range was only slightly, but significantly, expanded ($P \leq 0.001$, all animals). However, at the ends of these saccades (*column 3*), the torsional variance was increased further ($P \leq 0.001$, all animals) and by a larger step. If the function of these saccades components is to anticipate subsequent torsional components in slow phases, as hypothesized above, one might expect saccades during high head velocities (which tend to produce larger violations of Listing's law in the typical intersaccadic interval) to push torsion even more eccentrically. As shown in the *fourth column*, the subset of saccade ends where current head velocity was >150°/s did tend to land the eye at positions even more eccentric to the zero torsion zone ($P \leq 0.003$, all animals). However, after the subsequent slow phases (*column 5*), the eye was brought back to a torsional range almost as tight as the fixation range. Not surprisingly, the slow phase end range was very similar to the saccade start range because the two overlapped considerably during multiple-step gaze shifts (although *final* fixation points with the head motionless were included only in the former and starting points of the *1st* Eh saccade with the head moving were only included in the latter). More importantly, the torsional variance at the end of slow phases was reduced (highly significantly) compared with saccade ends in all three animals ($P < 2 \times 10^{-4}$ in *M1*, $P < 5 \times 10^{-9}$ in *M2*, $P < 6 \times 10^{-6}$ in *M3*). Thus unlike the head-fixed Listing's law, Donders' law of Eh was not obeyed *throughout* the overall gaze shift but only held during steady fixation (*column 1*) and transiently approximated toward the ends of interim slow phases (*column 5*).

3-D head trajectories

Figures 3 and 4 suggested that during steady fixations, the head-orientation range formed a pseudoplanar, twisted surface that required at least a second-order fit for adequate quantification. The latter is provided explicitly in Fig. 8, which shows the average parameters of second-order fits to the head-fixation range (averaged ± SD across all random-task measurements) for *animals M1* (*A*), *M2* (*B*), and *M3* (*C*).

Each parameter provides the dependence of Hs torsion on various combinations of horizontal and vertical position. The first parameter (a_1) measures the torsional shift of the range from the reference position, which was (not surprisingly) small (0.025, averaged across animals). The second parameter (a_2) indicates the dependence of torsion on vertical eye position, which was also small (−0.022, averaged across animals) and rather inconsistent. In comparison, the third parameter (a_3) was relatively large (−0.274, averaged across animals) and consistent both within and between animals. This term was significantly less than zero in all animals ($P < 3 \times 10^{-8}$ in *M1*, $P < 2 \times 10^{-14}$ in *M2*, $P < 10^{-6}$ in *M3*). This value represents the dependence of torsional head position on horizontal head position, and the illustrated negative value describes the upward (backward) tilt observable in the side view of the head fixation range illustrated in Fig. 3 (*E* and *H*), such that rightward positions tended to be more clockwise compared with leftward positions. The fourth parameter (a_4) was also negative on average. This negative value describes a curvature in the position vector range and signifies a tendency for the head to tilt counterclockwise when looking up or down (this is difficult to see in Fig. 3 because other terms are more dominant). Although a_4 was statistically significant in two of the three animals (*M1* and *M2*, $P < 0.05$), its mean value was relatively small

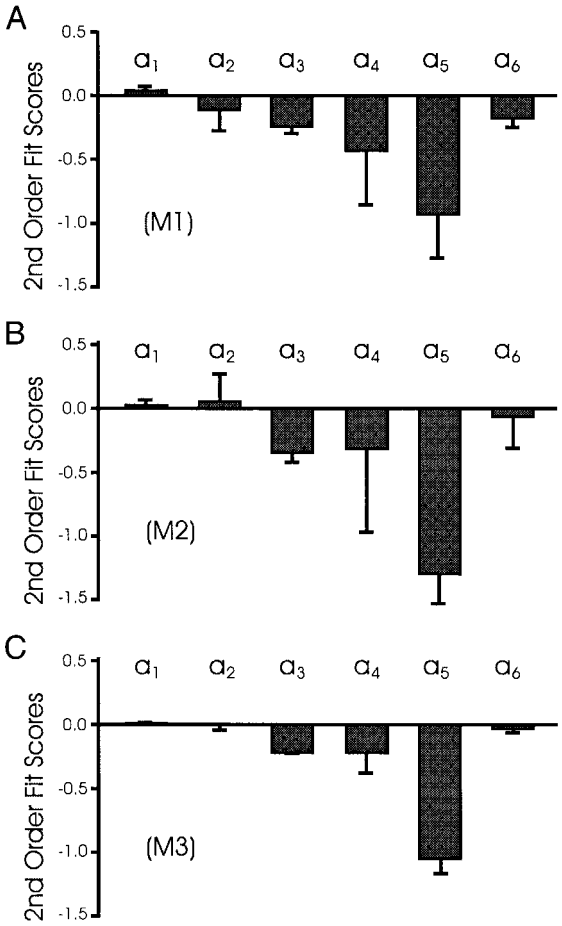

FIG. 8. Average parameters (a_1–a_6) of 2nd-order fits to 3-D head-orientation range in random saccade task. *A*: means and SDs across experiments in *animal M1*. *B*: means and SDs across experiments in *animal M2*. *C*: means and SDs across experiments in *animal M3*.

(−0.301, mean across animals) compared with its standard deviation between experiments (0.526, SD averaged across animals). The a_6 term, signifying curvature of torsion with horizontal eye position, was smaller again (−0.095, averaged across animals) and was only statistically significant in one animal ($P < 0.001$ in *M1*, $P \geq 0.257$ in *M2*, $P \geq 0.371$ in *M3*). Clearly, the most prominent term in the second-order head fits was the remaining a_5 parameter, the so-called ''twist score'' (Glen and Vilis 1992), which captures the bow-tie like twist illustrated in Fig. 3, *H* and *K*. As expected, this score was always negative (−1.104, averaged across animals), and was statistically significant across experiments in all animals ($P < 8 \times 10^{-6}$ in *M1*, $P < 2 \times 10^{-15}$ in *M2*, $P < 2 \times 10^{-5}$ in *M3*), confirming that the characteristic twist described above was consistent with the general trend.

Glenn and Vilis (1992) were the first to describe such negative twist scores in the human Hs range and to point out that this is the type of range that would be produced by a system acting like a set of Fick gimbals, i.e., a head-fixed horizontal axis (for vertical rotation) nested within a body- or space-fixed vertical axis (for horizontal rotation). They used a range-independent gimbal score (*Eq. 6*) to further quantify this twist, where −1.0 corresponds to zero torsion in a perfect Fick coordinate system, 0 corresponds to Listing's law, and 1.0 corresponds to zero torsion in a perfect Helmholtz coordinate system. The gimbal scores for our animals were −0.653 ± 0.136 (*M1*), −0.830 ± 0.086 (*M2*), and −0.567 ± 0.096 (*M3*) (mean ± SE across random-task experiments). This suggested a constraint on static head orientation during fixations that was intermediate between Listing's law and a perfect Fick system but somewhat closer to the latter.

However, because an infinite number of rotational axes can take the head between any two fixation points (Tweed and Vilis 1990), it was not clear from this data, or the previously published human fixation data (Glenn and Vilis 1992; Radau et al. 1994), whether the head actually rotates like Fick gimbals during movements. To answer this question, it was necessary to directly examine the instantaneous axes of head rotation during gaze shifts. To begin at a relatively simple level, purely vertical or horizontal head movements first were examined. Figure 9 illustrates the typically observed behavior, showing the instantaneous axes of rotation (angular velocities) used for various vertical (*A*) and horizontal (*B*) head movements from various initial head orientations. Figure 9*A* shows five downward head rotations at five different horizontal head positions. As indicated by the head caricatures, the data are projected onto the horizontal plane from a perspective above the head. The cartoons in Fig. 9*A* illustrate two examples where - - → indicates the average pointing directions of the head in the first and fifth movement, and — indicates the average axes of rotation.

In the main part of Fig. 9*A*, head position is indicated by five groups of head direction vectors (dark points labeled 1–5) that are joined to the origin by - - - (because these downward arcing vector tips are viewed from above, they do not appear to change very much during the movement). Also shown are five ''velocity loops'' (labeled 1–5), where the individual points (□/■) provide the instantaneous axis and angular speed of

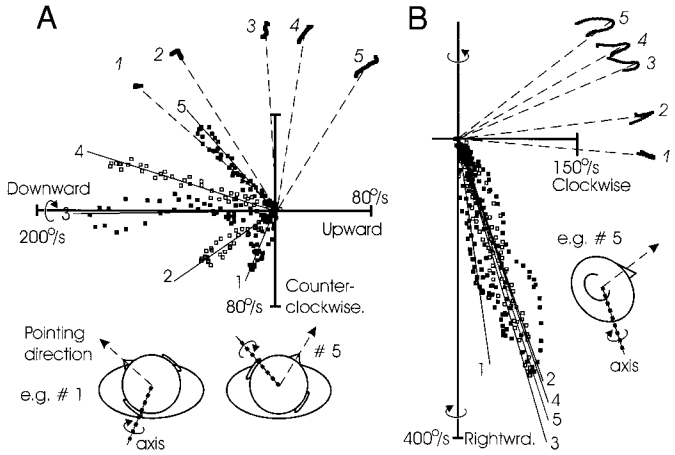

FIG. 9. Fick-like nature of head angular velocity axes during movements selected from randomly directed gaze shifts. *A*: axes of 5 downward head movements at 5 different horizontal head positions viewed from above in space-fixed orthogonal coordinates. For each movement, individual angular velocity vectors (■, movements 1, 3, and 5; □, movements 2 and 4) are provided, forming accelerating/decelerating loops, along with the average axis (—), numbered 1–5. Also shown are the tips of the corresponding 2-D head ''pointing direction vectors'' during these same movements, numbered 1–5 and joined to the origin by - - -. Head caricatures for examples 1 and 5 indicate that the horizontal axis for vertical head rotation remains nearly head-fixed. *B*: axes of 5 rightward head movements at 5 different vertical head positions viewed from the side in space-fixed orthogonal coordinates. Same conventions as *A* but now the vertical axis for horizontal head movement remains relatively fixed in space, independent of head position. *Animal M1*.

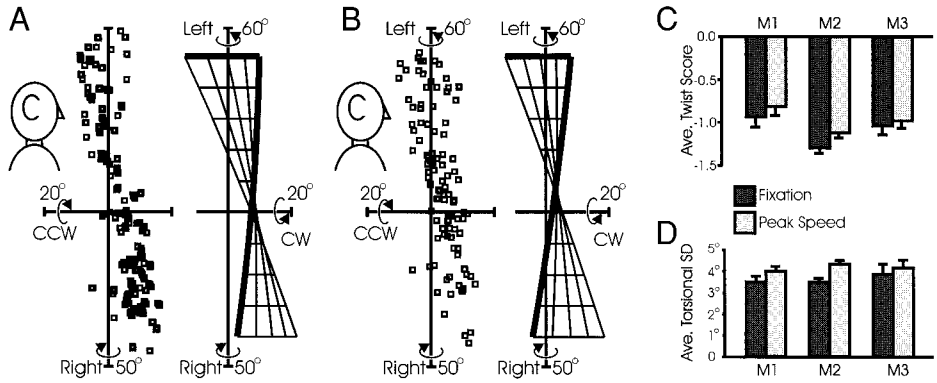

FIG. 10. Comparison of 3-D head orientation range during fixation (*A*) and during peak head velocities (*B*). *A*: side view of control head fixation range, and 2nd-order surface fit to same data. (See Fig. legend 3 for description). Random task in *animal M1*. *B*: same experiment, but data computed from head positions at peak head velocities of each movement. *C*: quantitative comparison of 2nd-order twist score (a_5) of head during fixation and peak head velocity. Averages and SEs across all experiments are shown for all 3 animals. *D*: quantitative comparison of torsional standard deviations of head to 2nd-order surface fit during fixation and peak head velocity. Averages and SEs across all experiments are shown for all 3 animals.

head rotation. The numbering system indicates the correspondence between position and velocity for each of five movements. In each movement, the velocity vector started at zero and then grew (accelerated) to some maximum value closely along some constantly oriented axis of rotation (—) and then shank along this axis back down to zero, thereby forming a narrow loop. Note that as the head pointing direction proceeds from left to right (1–5) across the five different movements, the axes of rotation (1–5) for the downward head movements stay in the horizontal plane but similarly rotate stepwise to the right, such that the head axis stays close to orthogonal to the head pointing vector in each case. Furthermore, the axes of rotation remained roughly constant throughout each movement. This dynamic behavior was very much like the rotations that occur about the horizontal axis in a set of Fick gimbals, where this nested axis initially has been rotated horizontally to different degrees about a vertical axis.

Figure 9*B* uses similar conventions but now shows a side view of the vertical velocity loops for five rightward head rotations (1–5) with the head at five different vertical elevations as shown again by the five groups of corresponding head pointing vectors (1–5). The latter form little semicircles because they represent the arcing tips of a vector that was swinging horizontally, and the view of these arcs is not perfectly edge-on. In general, the velocity vertical axes did not align with the gravity vector (the vertical coordinate axis in the plot) but rather showed a consistent upward tilt so that rightward rotations had clockwise components (Fig. 9*B*) and similarly leftward rotations had counterclockwise components (see Fig. 12*A*). More importantly, the five sets of velocity loops formed a compact, overlapping set of data points. There was little or no systematic tilting of these five axes with the vertical elevation of the head. Furthermore the orientation of the axis of each rotation remained roughly constant throughout the trajectory (this is further illustrated below in Fig. 12). Thus again, these head rotations strongly resembled those produced by telescope-like Fick gimbals, where the vertical axis for horizontal rotation remained fixed with respect to space throughout the movement, despite various initial displacements about the horizontal axis.

Taken together, Fig. 9, *A* and *B*, suggests that the Fick-like constraint observed in the head-fixation range (Fig. 3, *H* and *K*) results because the head does indeed rotate about axes like the nested coordinates in Fick gimbals during rotations. These two figures (3 and 9) are linked as follows. First, the upward tilt in the fixed vertical axis (Fig. 9*B*) accounted for the upward (backward) tilt in the position ranges of Fig. 3, *E* and *H*, and the corresponding negative a_3 term in Fig. 8. For example, rotation about this tilted axis caused head position to deviate clockwise during rightward movements. Second, and more importantly, the Fick-like nesting of the axes in Fig. 9 gave rise to the bow-tie shape in the fixation range (Fig. 3*H*). For example, during a downward movement with the head rotated to the left (e.g., Fig. 9*A, 1*), the ''horizontal'' axis (for vertical rotation) was rotated similarly to the left so that it then almost aligned with the *torsional* axis in space-fixed orthogonal coordinates. Thus at this position, downward rotation in Fick coordinates was almost the same as counterclockwise rotation in space-fixed orthogonal coordinates. This explains why downward-leftward positions had a relative counterclockwise twist in the fixed orthogonal coordinates used in Fig. 3*H*. Similar factors explain the torsional twists at the other corners of the Fick surface (Fig. 3*H*).

On the basis of these velocity data, it would appear that the Fick constraint on head position should hold during movements just as Listing's law holds fairly well during head-fixed saccades (Ferman et al. 1987b; Straumann et al. 1995; Tweed and Vilis 1990; Tweed et al. 1994). To quantitatively test this hypothesis, we reexamined the head-orientation ranges during the random-gaze task, now focusing on the range during movement. Figure 10 shows such head-orientation ranges *during* random-gaze shifts and their 2-D surfaces of best fit. Figure 10*A* shows head positions during steady fixations as a control, whereas *B* shows head positions that were selected at the point in time when peak velocity occurred for each head movement. From this example (*A* vs. *B*), it would appear that the Fick-like twist remained even during movements. This is quantified in Fig. 10*C*, which compares the average twist scores (±SE across experiments) fit to fixation data (as in *A*) versus average twist scores fit to the head positions at the time of peak head velocity (as in *B*) across all random-task experiments in each monkey. It would appear that the twist scores remained relatively constant in both conditions, showing only a slight reduction during peak head velocities. This reduction was statis-

tically significant in *animal M2* ($P \leq 0.001$) but not *animal M1* ($P \geq 0.15$) or *M3* ($P \geq 0.21$).

Figure 10*D* then shows the average torsional standard deviations ($\pm$SE) from these fits, again comparing fixation data versus position data collected at peak head velocities. All three animals showed a modest (mean 15%) increase in torsional variance during peak head velocities. This increase was statistically significant in two of the three animals ($P \leq 0.012$ in *M1*, $P \leq 0.0005$ in *M2*, $P \geq 0.113$ in *M3*). Thus it appeared that the Donders' law of the head was relaxed only slightly during head movements, at least when averaged across *all* types of movements in the random task.

One explanation for the small but consistent increase in variance of head torsion during head movements could be random biological noise. However, there is still reason to hypothesize that some specific movements were not Fick-like during the movement. Fick-like movement trajectories like the vertical and horizontal rotations shown in Fig. 9 may have dominated the dynamic behavior in the random task (Fig. 10*B*), masking a less frequent, dynamically non-Fick behavior. In particular, we have not yet addressed the behavior of the head during large *oblique* movements. The potential complication here is that in a mechanical Fick system, the horizontal component of an oblique axis would be position *dependent*, whereas the vertical component would be position *independent.* Thus as described in INTRODUCTION, a mechanical Fick system (or any other system that maintains zero torsion in Fick coordinates) must produce specific nonconstant curvatures in the rotation axis during large oblique movements. A system that did not produce such curved trajectories would therefore not obey Donders' law *during* large oblique movements even if the endpoints did obey Donders' law.

Consider the hypothetical situation depicted in Fig. 11, *A–D, top. A* depicts our paradigm where the head rotates in an ''hourglass'' pattern, consistently reproducing large oblique movements but without repetitive back-and-forth motion (to be addressed in a subsequent section) or circular patterns that might lead to accumulation of torsion (Tweed and Vilis 1992). Only head position vectors are depicted, using the right-hand rule, as viewed from behind (*left*) and from the side (*remaining columns*). Assume for the moment that Hs conforms to the ideal Fick constraint during fixation as depicted schematically in Fig. 11*B.* In this case, a large oblique rotation must take the head between similarly eccentric torsional orientations. For example, the rotation from down-right (DR) to up-left (UL) begins from a clockwise orientation in space-fixed orthogonal coordinates and ends at a similar clockwise orientation. The question is, what path will it take?

If head orientation was constrained to the Fick surface mechanically, or maintained in the Fick surface by a neural rule that operates at all times during the movement, then it would follow the 3-D trajectories illustrated in Fig. 11*C.* It could not pass through the center of the range without crossing a zero-torsion line on the Fick surface. However, if the Fick strategy was preprogrammed before movements such that the control system only really cared about terminating in the Fick surface, it might accept transient violations in the Fick strategy to take the more direct paths illustrated schematically in Fig. 11*D*.

Figure 11, *E–G,* shows the experimental result of the test described above. Other than the irrelevant backward tilt of

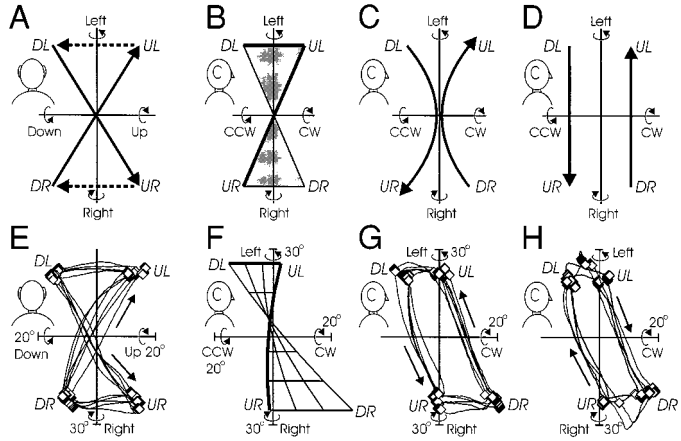

FIG. 11. Oblique head movement test for a Fick gimbal operator. *Top*: paradigm and theory. *A*: hourglass paradigm designed to provide consistent oblique head movements without repetition effects shown in previous figure. Monkey makes gaze shifts between 4 corners (shown in right-hand rule convention, behind view), causing the head to move in the indicated pattern. UL, up-left position; DR, down-right position. *B*: idealized Fick gimbal surface, shown in side view (torsion vs. horizontal). To go between opposite corners without departing from this surface (e.g., DR-UL), the head must pass through a 0-torsion zone. *C*: theory 1: Fick gimbal strategy mechanical or within a neural feedback loop that operates during movement. Oblique head movements (e.g., DR-UL) stay within ideal Fick range. *D*: theory 2: Fick gimbal strategy provided by a feed-forward operator that computes desired final head position but is not concerned with intermediate positions. Oblique head movements pass from 1 torsional corner to another torsional corner without passing through 0 torsion zone, thus departing from Fick surface. *Bottom*: actual data from *animal M2. E*: 5 repetitions of head trajectory in task corresponding to *A.* Behind view, right-hand rule. *F*: side view of 2nd-order fit to head fixation data from this experiment. See Fig. legend 3 for detailed description. *G*: torsional trajectories of the head in this task. *H*: torsional trajectories in complimentary task, where head follows a similar path but in the opposite direction.

the Fick-like range (Fig. 11*F*), the data closely emulated the ideal test. From the behind view (Fig. 11*E*), the oblique head-position trajectories sometimes showed some slight and variable curvatures as observed in human head movements (Tweed et al. 1995). However, in the side view critical to the test (Fig. 11*G*), the head followed remarkably straight trajectories directly from one torsionally eccentric corner to the next. This was consistent in other variations of the hourglass paradigm, such as that shown in Fig. 11*H*, which depicts the same task only with gaze/head position rotating around the same sequence in the opposite direction. Clearly the control system transiently abandoned the zero-torsion (in Fick coordinates) fixation range during these oblique trajectories in favor of a more direct trajectory, supporting the theory illustrated in Fig. 11*D.*

Task-dependent modifications in the head's Fick strategy

If the observed constraints on head orientation and axes during gaze shifts were neural in origin, as they appeared to be in Fig. 11, then they might show some capacity for plasticity or task dependence. Here we describe two circumstances in which such task dependencies indeed were observed. First, Tweed and Vilis (1992) reported that during repetitive back-and-forth movements, the axes of head rotation showed a tendency to tilt toward the axis perpendicular to the plane containing the head direction vectors such that the angle of rotation was minimized. We tested this by having *monkeys M1* and *M2* perform repet-

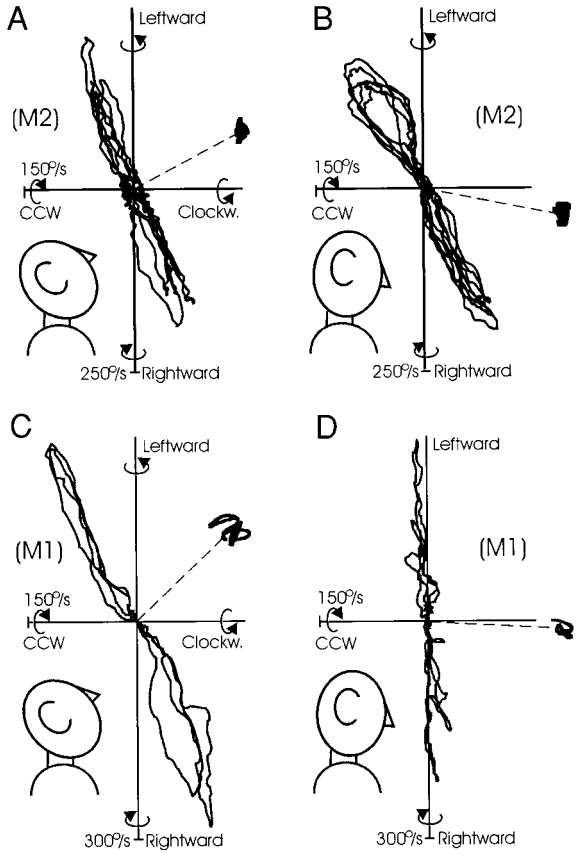

FIG. 12. Partial break-down of the Fick constraint during repetitive horizontal head movements in *animal M1* but not *animal M2*. Angular velocity vectors are joined in lines forming continuous loops and viewed from the side in space coordinates. Two-dimensional head-direction vectors also are shown, joined to the origin by - - -. *Left*: repetitive left/right movements with the head pointed up. *Right*: repetitive left-right movements with the head pointed down. *A* and *B*: *animal M2* (negative effect). Velocity axes for 5 sequential left-right repetitions (in each direction) are shown at both levels. *C* and *D*: *animal M1* (positive effect). Axes for the 2nd and 3rd left-right movement pairs in a repetitive sequence are shown at both levels.

itive back-and-forth vertical or horizontal movements at various positions (again, *M3* refused to comply with these task demands). The case where horizontal movements were repeated at different vertical levels was a more dramatic test of this effect because it would tend to violate the normal space-fixed character of the vertical rotation axis.

Figure 12 shows the results of this test in both monkeys. Angular velocity loops during repetitive horizontal rotations are viewed from the side perspective in each panel along with the 2-D directional vectors of the head (– – –). *Left panels* show the case where gaze and Hs were tilted upward, whereas *right panels* show the case where gaze and Hs were tilted downward. Unfortunately, the two monkeys showed two different results. Figure 12, *top*, (*A* and *B*), shows the effect typically observed in *animal M2*. This animal did not show the minimum rotation effect observed in humans. Even after five (as illustrated) or more movement repetitions in each direction, the axis of rotation remained remarkably fixed in the Fick-like fashion. However, *animal M1* (*C* and *D*) did show the minimum rotation effect reported in humans (Tweed and Vilis 1992). By the second and third horizontal repetition (as illustrated), the head axis already had tilted maximally toward a point quasiorthogonal to the head direction vector. Thus the use of this strategy appeared to be subject dependent.

For a more specific test of the task dependency of these constraints, we used a second paradigm. In this case, the fixation range of the random task was reexamined while two trained animals (*M1* and *M2*) performed gaze shifts wearing opaque plastic goggles with only a small hole positioned over the center of the right eye (Crawford and Guitton 1997b). This reduced the visual range to a head-fixed monocular zone of $\pm 4°$, which removed several normal visual task constraints (discussed in the next section) and forced the head to become the primary mover of gaze. Therefore we tentatively hypothesized that the head might behave more like Eh in this task, i.e., obey Listing's law. Remarkably, this simplistic hypothesis proved to be essentially correct.

Figure 13 illustrates the results of this test. Note that in this figure, only random-task fixation points are considered, which in previous sections were confined exclusively to the twisted Fick-like surface. Figure 13*A* shows the second-order fit to a control head range recorded just before putting on the goggles, revealing the typical Fick-like twist. Figure 13*B* then shows the analogous fixation range of head-orientation vectors recorded while the pretrained animal made randomly directed movements immediately after the goggles were put in place. As in all other experiments, this produced a slight clockwise shift in head posture, toward the side with the aperture. More importantly, the second-order fit to the range flattened out to closely resemble similar fits to Eh position during saccades (Crawford and Vilis 1991). Figure 13*C* quantifies this effect by showing the average (and SEs across experiments) twist scores (term a_5, *Eq. 5*) during the random goggle task against the analogous control scores, in both trained animals. On average (across the means of the 2 animals) the goggles caused a reduction in the head twist score to only 31.4% of its normal value. This reduction was statistically significant in both *M1* ($P \leq 0.011$) and *M2* ($P \leq 0.0005$).

Moreover, the variance of the head twist score increased substantially during the goggle task, particularly in *animal M1*. Because this variability might prove to be important in interpreting the goggle effect, several further examples of second-order surface fits to individual experiments have been provided (Fig. 13, *D–F*). During the goggle task, *animal M1* sometimes reproduced the normal Fick-like fixation range (Fig. 13*D*) but sometimes produced the dramatically opposite twist consistent with Helmholtz coordinates (Fig. 13*F*). During other goggle experiments, *M1* (and *M2*) produced ranges intermediate between these extremes that were either flattened (Fig. 13*B*) or curved with little twist (Fig. 13*E*).

DISCUSSION

The general impact of this experiment can be summarized in three statements. First, our description of the neural constraints on orientations of Es, Hs, and Eh during visual fixations following head-free gaze saccades in the monkey largely confirm similar constraints observed in humans (Glenn and Vilis 1992; Radau et al. 1994). Such confirmation is useful because of the inherent stability of coil signals in surgically implanted animals as opposed to human search coil measurements. More importantly, it suggests that (despite certain head-neck anatomic differences) the monkey is an appropriate animal model

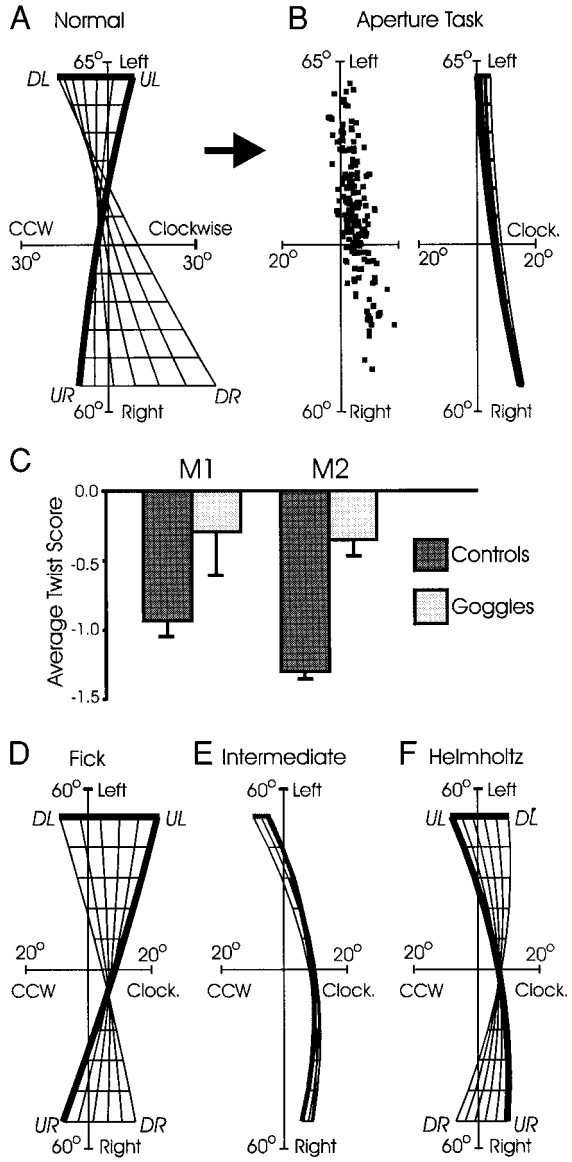

FIG. 13. Collapse of curved 3-D head surface toward a Listing's plane during pin-hole goggle task. *A*: 2nd-order surface fit to control head fixation range in random task, showing typical Fick twist. (See Fig. legend 4 for a detailed description.) *Animal M2. B*: head fixation range during subsequent random task in *M2* with pin-hole goggles together with 2nd-order fit to this range, revealing a planar organization. *C*: quantitative comparison of 2nd-order Fick scores (a_S) of control random head-fixation range and range with pin-hole goggles. Averages and SEs across all experiments are shown for both animals. *C*: 3 additional surface fits to random pin-hole goggle data in *animal M1*, graphically showing wide variations from a Fick-like twist, to another intermediate, to a Helmholtz-like twist.

to investigate the physiological mechanisms of this behavior, and thereby test computational models that have arisen from experiments with humans (i.e., Tweed 1997). Second, our analysis of orientation and velocity trajectories in Eh and Hs address several issues pertaining to 3-D gaze control that were either left unaddressed or only inferred indirectly in previous 3-D studies. In particular, we have shown that Eh saccades anticipate torsional violations of Listing's law to land final Eh position at zero torsion and that Hs dynamically acts like a Fick gimbal *during* horizontal and vertical movements but not during oblique movements. Finally, we have shown for the first time that the head-fixation constraint is task dependent and modifiable by visual input. Each of these observations has important implications for understanding the neural control of gaze direction in 3-D space.

Constraints on Es, Hs, and Eh during visual fixation: implications for perception and control

Listing's law of Eh (with the head stationary) is the quintessential motor synergy in the sense that it is obeyed with a high degree of precision (Ferman et al. 1987; Tweed and Vilis 1990; Tweed et al. 1994), it has been known for more than a century (Helmholtz 1867), and it subsequently has engendered considerable research and controversy (reviewed in Crawford and Vilis 1995; Hepp et al. 1994; Quaia and Optican 1998). Surprisingly, it is still not clear which factors determine this particular implementation of Donders' law, e.g., as opposed to the Fick strategy observed in Hs. In the 19th century both Hering (1868) and Helmholtz (1867) formulated arguments for Listing's law based on the assumption that it provided certain geometric constancies between the retina and the external world. Such arguments assume that Listing's law (i.e., a planar range of eye position vectors) holds with a high degree of precision for eye orientations *in space* when the head is free to move in a natural fashion. It originally appeared that both Es and Hs do obey Listing's law at least over a relatively central range of positions (Straumann et al. 1991; Tweed and Vilis 1992). However, more recent data from humans (Glenn and Vilis 1992; Radau et al. 1994), and now monkeys, calls this into question.

First, even for a central target, the torsional range of Es around the line of sight is highly variable (Fig. 2) (Radau et al. 1994). Second, over a larger 2-D gaze excursion, the 3-D orientation range of Es is not planar but rather twisted like the range associated with Fick gimbals (Fig. 3) (Glenn and Vilis 1992; Radau et al. 1994). Indeed, even with a third-order fit, the torsional variance (SD) of our Es data was consistently larger (average 3.55°) than that of our Eh data (average 1.87°). Even though we analyzed a much more variable and random 2-D Es/Hs range compared with those used in the human experiments, the former is almost identical to the analogous human Es data (Radau et al. 1994), whereas the latter is slightly smaller than the human Eh data (perhaps simply due to minor experimental slippage in human search coil lenses). The torsional SD of our Hs data was slightly smaller (average 3.10°) than our Es variance but was considerably smaller than the corresponding human Hs value of 4.75° (Radau et al. 1994). Note that the latter value was cut to less than half when recomputed relative to the chest, which we could not do for technical reasons. These data suggest that it is the 3-D orientations of Eh and Hs (or more likely head-relative-to-chest) that are constrained physiologically and that the apparent constraint on Es is only the geometric byproduct of the other two constraints (Radau et al. 1994).

This by no means suggests that the observed constraints do not have important implications for perception and the interpretation of visual information for motor control. Even considering the high torsional variance observed in Es compared with Eh, the behavioral range of Es torsion is still relatively small compared with its potential mechanical range (about $\pm 90°$ in an upright primate). Moreover, the Fick-like Es range

keeps the para-foveal horizontal meridian of the eye in better alignment with the horizon than does Listing's law (Glenn and Vilis 1992; Klier and Crawford 1998). These constraints are relevant to the problem of space constancy in high-level object recognition because they reduce the number of retinal perspectives required to develop object-centered representations of natural visual targets, which themselves are normally earth-oriented (e.g., Marr 1982). Similarly, although information about 3-D eye and head orientation may be used to interpret the spatial content of retinal input, this process probably depends on continual visuomotor calibration for various combinations of eye/head position (Crawford and Guitton 1997a; Haustein and Mittelstaedt 1990; Helmholtz 1867; Klier and Crawford 1998). Therefore the observed constraints on Eh, Hs, and Es orientation probably reduce the computational load for high-level object recognition and egocentric localization. This is consistent with the observation that accurate spatial perception of the roll-tilt of visual stimuli breaks down with large Es torsion (e.g., Wade and Curthoys 1997).

3-D Eye-in-head constraint and coordination of Eh saccades with slow phases

The previous section suggested that physiological constraints on eye orientation are controlled at the level of Eh rather than Es. Such a constraint is necessary for the oculomotor system to convert its 2-D visual inputs (which only specify desired gaze direction) into actuated 3-D eye positions in an orderly fashion. In other words, Donders' law solves the degrees-of-freedom problem (Crawford and Vilis 1995). Considerable controversy has persisted over the question of whether the Eh is constrained solely by its musculature to obey Donders' law during saccades or whether a specific neural implementation is required (e.g., Crawford and Guitton 1997; Crawford and Vilis 1991; Hepp 1994; Quaia and Optican 1998; Raphan 1997, 1998; Tweed and Vilis 1990; Tweed et al. 1994; Van Opstal et al. 1996). This mostly has been studied in the head-fixed preparation, where the eye obeys Listing's law. However, it is the range of eye orientations during *head-free* fixations that will be most important for vision in its natural element.

To address these issues, our first goal was to determine the shape (if possible) and thickness of the Eh fixation range. Unfortunately the 2-D fixation range of Eh was much smaller than the corresponding Es and Hs ranges. As a result, it is difficult to be confident in higher-order terms describing any nonplanar aspects of the shape of the Eh fixation range for the same reason that it is difficult to fit a line to a small circular blob of points in an *x-y* scatter plot: the range of the independent variables was insufficient to distinguish between higher-order terms that would only become quantitatively important at eccentric positions. In a previous paper, Radau et al. (1994) statistically compared the goodness of fit of first-, second-, and third-order fits to the Eh fixation range during head-free gaze saccades across seven human subjects and concluded that the Eh range was not significantly different from a plane. We could not take this approach because of the insufficient number of animal subjects. However, our observations were consistent with their conclusions, i.e., despite the statistical improvement in torsional variance with higher-order fits to the Eh data, these improvements were not impressive on visual inspection of the data (Fig. 4), and the nonplanar terms of the fit were highly variable. Therefore we conclude that, although the monkey Eh fixation range may or may not show some slight quantitative curvature, there is no practical advantage in distinguishing these ranges from a plane. Moreover, these head-*free* fixation ranges were only slightly thicker in one animal (*M3*) and only about twice as thick in the other two animals compared with the torsional range reported for head-*fixed* primates (Crawford and Vilis 1991; Straumann 1991; Tweed et al. 1990). This is remarkable considering the magnitude of head motion occurring between these fixations.[1]

We therefore focused on the mechanisms that maintained this relatively tight torsional fixation range despite transient large torsional ''violations of Listing's law'' observed during various points in the multistep gaze saccade. It was observed that Eh saccades were driving eye position away from the quasiplanar fixation plane, such that subsequent slow phases brought the eye back into the plane with particular accuracy during the final slow phase that preceded termination of the associated head movement. This complex goal-directed torsional behavior contradicts the idea that Listing's law results from a fixed internal projection of visual representations onto a 2-D plane of saccade vectors (Raphan 1997, 1998). Instead, it supports the idea that Listing's law is upheld by a specific neural mechanism that (in effect) selects a desired torsional eye position in Listing's plane[2] (Crawford and Vilis 1991; Tweed 1997; Van Opstal et al. 1996).

The inherent difficulty with implementing such a mechanism during head-free gaze saccades is that they *end* with movements (slow phases) that are not themselves purposeful, aimed movements but rather are dictated by head rotation kinematics. Thus it would be up to the Eh saccade generator to somehow *anticipate* these subsequent movements (there seems to be no other function to these rapid torsional movements because they do not affect gaze direction). Furthermore as described in more detail elsewhere (Crawford and Vilis 1991; Smith and Crawford 1998), the kinematic effects of slow phases on torsional position can only be predicted from knowledge of both head velocity and eye position. Therefore to land Eh on a final desired 3-D orientation, the head-free Eh saccade generator would have to employ an algorithm that accounts for both Eh position and anticipated head motion (Crawford and Vilis 1991). In a recent model, Tweed (1997) implemented such an algorithm with the use of desired 3-D Es and Eh orientation commands such that simulated head-free gaze saccades did ultimately land Eh position within Listing's plane, as we have now confirmed in the monkey.

[1] Part of the increase in the head-free Eh fixation range compared with the head-fixed range may have been due to dependencies of static eye torsion on static head orientation. For example, the systematic clockwise/counterclockwise deviation of head orientations during right/left head positions, respectively, may have induced a small ocular counter-roll. This static counter-roll could cause the Eh fixation plane to apparently tilt or widen, depending on the variability between eye and head position for a given gaze direction. Moreover, even zero-roll horizontal head orientations have been shown to affect the orientation of Listing's plane relative to the head (Misslisch et al. 1998) possibly leading to similar widening effects during our random task.

[2] This does not contradict the idea that muscular position-dependencies might facilitate and simplify the neural maintenance of Listing's law when the head is fixed, where eye position remains within Listing's plane (Crawford and Guitton 1997; Demer et al. 1995; Quaia and Optican 1998; Raphan 1998).

At first thought, it might seem like computational overkill to employ such a complex mechanism to anticipate violations of Listing's law. However, consider the alternatives: without a torsional corrective mechanism, huge (>20°) Eh and Es torsions would arise during a single multiple-step gaze shift (as extrapolated in Fig. 6), which could disrupt space-centered vision, as discussed earlier, and disrupt stereo vision in a headcentric frame (Howard and Zacher 1991). Second, if this corrective mechanism was triggered only *after* the torsional slow phase, it then would transiently disrupt vision at the end of the gaze shift, when visual stability is most critical. Moreover, these mechanisms probably do not only pertain to torsional control. In the current experiment, there was no special distinction among the horizontal, vertical, and torsional aspects of this anticipatory behavior (e.g., Figs. 5–7) except that the torsional fixation range was considerably more restricted than the 2-D fixation range.

Perhaps the most dramatic confirmation of this effect was described in our previous report (Crawford and Guitton 1997b), in which *animals M1* and *M2*, after training on the original pin-hole aperture (described in the current study), were then unable (initially) to direct saccades toward a new, slightly displaced central aperture. Instead, regardless of starting position, Eh saccades directed the eye toward a location appropriate for the subsequent slow phases to bring the eye back toward the learned 2-D location of the (now occluded) original aperture. The latter strongly suggests that the vertical and horizontal components of final post-VOR Eh position also are preprogrammed, using an algorithm such as that described earlier (Tweed 1997). This converging evidence suggests a mechanism whereby Eh saccades account for initial eye position, desired target direction, and anticipated head movement to select each component of desired final 3-D Eh orientation within some internally delimited central range. In terms of 2-D direction, this Eh fixation range was flattened in the horizontal dimension (Freedman and Sparks 1987; Glen and Vilis 1992), whereas the torsional degree of freedom was even more limited to a range approximating Listing's plane.

Fick operator for the head?

Compared with the oculomotor system, which must point an easily defined 2-D visual axis toward targets, the job of the head-control system in gaze shifts is more difficult to state in quantitative terms. Perhaps it is best stated that the head, in its capacity as the platform for the oculomotor system, must be directed such that in the end, the target is within the internally delimited head-free oculomotor fixation range discussed earlier. Thus instead of a single vector (the visual axis), the head must rotate a binocular pair of 2-D Eh fixation ranges toward the target (think of a head-fixed flashlight, where 2-D Eh direction can only end up within the spread of light). This gives rise to two further degrees-of-freedom problems in choosing head orientation.

First, because a target potentially still can be acquired (by the eye) at an infinite number of points within the headcentric Eh fixation zone, the associated range of 2-D head pointing directions is not severely limited by this ocular fixation range (Radau et al. 1994; Tweed 1997). The data suggest that the head probably does not use all of its allowable range of freedom in thus acquiring targets (if it did, then the associated 2-D Eh range for one target would be as big as the *complete* Eh range), and yet it still showed much more 2-D variation than gaze direction for a single target (Fig. 2). This suggests that the oculomotor ''fixation range'' described earlier is really the amalgamation of smaller zones for each body-centric target direction, further limiting the allowable range of 2-D ''pointing'' directions of the head for each target. At the extreme, a unique desired head position for a given target could be selected by first computing the desired final Eh position (Tweed 1997), but this does not account for the variability observed here in final head positions. However, the possible range of eye-head combinations for a given target probably is constrained further by the combination used at the previous fixation point (Becker and Jürgens 1992; Freedman and Sparks 1997; Fuller 1996; Goossens and Van Opstal 1997) and the behavioral context (Crawford and Guitton 1997b).

The second degrees-of-freedom problem in head control is like that of the eye, i.e., even with a very narrow headcentric range of desired facing directions, the head potentially could orient about the head-centric torsional axis passing through the center of this range through any arbitrary angle and still have gaze acquire the target. Again, although Hs torsional variance was slightly larger than Eh torsional variance, over a large range it was clearly limited compared with the possible mechanical range of torsional head motion. Moreover, this range formed a consistent shape (Fig. 3) similar to that observed in humans (Glenn and Vilis 1992; Radau et al. 1994). However, the vertical axis of the monkey range was tilted from the more gravity-aligned head position range reported in humans (Misslisch et al. 1994b), even in *animal M3,* which was allowed to slouch in a self-selected posture. More importantly, the shape of this range was twisted like the range produced by Fick gimbals when torsion (in Fick coordinates) is held at zero, i.e., rotations about a headcentric torsional axis indeed were minimized. Our more precise quantitative analysis suggested that this range was intermediate between a pure Fick constraint and a perfect Listing's law but somewhat closer to the ideal Fick rule than the ranges reported for humans (Glenn and Vilis 1992).

In as much as this range is violated easily by voluntary effort and is not determined by 2-D retinal input, it must be implemented by the neural equivalent of a ''Fick operator'' (Tweed 1997). (This does not necessarily imply that this operator is located in a compact nucleus or in any easily identifiable pattern of signals.) Moreover, the observation that the head range is modified readily to a more Listing-like plane by restricting visual input suggests that this range optimizes task constraints rather than purely mechanical constraints (Radau et al. 1994; Theeuwen et al. 1993). This task dependence may explain why monkeys and humans show such similar Hs behavior, despite differences in the gross anatomy of their foramen magnum and neck posture.

In this paper, we tried to address the nature of this Fick operator by examining it under various conditions of normal fixation and adapted fixation and during rotations about various axes. This is relevant both to determining the algorithm used by the Fick operator and determining the behavioral parameters that it might be optimizing (Glenn and Vilis 1992). From the normal random fixation data and from the axes of rotation during cardinal horizontal or vertical move-

ments, it appeared that both the static and dynamic head ranges were remarkably Fick-like, i.e., it was difficult to distinguish whether position or velocity was being optimized. However, during oblique head movements, there was a clear trend to abandon the Fick constraint during the movement to take the most direct path from one position to another position in the Fick ''surface.'' Besides demonstrating again that the head's Fick strategy is not a mechanical constraint, this has the remarkable implication that the Fick operator does not operate within a head motor feedback loop but rather only chooses a final *desired head orientation*. (The implications of this for feedback control of gaze direction will be considered in a later section).

Any one desired head orientation can be reached from a given initial position by an infinite number of rotational axes, and the data suggest that the neural algorithm used to select these axes is rather complex. For example, if the head always rotated about the axis of minimum rotation (orthogonal to the plane of the initial and final pointing vectors), then it would not rotate in the observed fashion about a fixed vertical axis during horizontal gaze shifts. Thus during randomly directed, normal head-free gaze shifts, the static and dynamic constraints on head position might be characterized by the following rule: the head-control system compares current and desired head position and then chooses the unique (constantly oriented) axis of rotation that most closely fits the Fick gimbal strategy. This would explain why horizontal and vertical rotations remain Fick-like throughout the movement because in these situations the desired Hs orientation always can be reached by rotating about a constant axis in Fick coordinates. However, because oblique movements require *nonconstant* axes to maintain Fick torsion at zero, the aforementioned rule only could approximate this ideal curved trajectory with a single fixed axis, which would lead to the transient deviations from the Fick surface described earlier. Unfortunately, even this rule broke down during repetitive horizontal gaze shifts in *animal M1*, which showed a tendency to optimize the vertical axis in an energy efficient, non-Fick fashion, like the minimum rotation strategy observed in human head movements (Tweed and Vilis 1992) and to a lesser degree in some human eye movements (DeSouza et al. 1997). Therefore, it is probably more accurate to call the Fick operator a ''Donders' operator,'' whose function is to choose the best 3-D trajectory for a given behavioral context.

These data thus suggest that the 3-D head-control strategy is optimized for a number of motor and possibly sensory factors. Perhaps the best question to focus on next is why the Fick strategy is used during fixation. Our pin-hole goggle task would tend to suggest that there is something about normal task constraints on head movement that maintain the use of a Fick strategy during fixations. Parenthetically, the increased head range in this task would not artificially lead to a lower twist score because twist scores tend to be underestimated for smaller ranges. The flattening of the head range during this task might indicate that Listing's law was more optimal for the new eye-like role of the head in directing gaze or it might simply indicate a tendency to slip toward a default strategy during the removal of some key task constraint. The increased variability in the twist score in this task might tend to support the latter idea.[3] For example, this constraint could depend on peripheral vision or alignment of the two seeing eyes with the horizon (Glenn and Vilis 1992), cues that were absent with the pin-hole goggles. In any case, our result shows that, contrary to a previous suggestion (Radau et al. 1994; Theeuwen et al. 1993), the Fick strategy does not appear to optimize purely mechanical parameters. Further variations of this experiment might precisely pin down the relevant constraint, but this is beyond the scope of the current paper.

Another important factor that this study could not address is the translational component of head movement. Because our animals showed the same orientation constraints whether the head was allowed to freely translate (*animal M3*) or not (*M1* and *M2*), additional measurement of head translation should *not* invalidate our current observations on orientation. However, measurement of head translations is important for targets closer to the eye than those that we examined because they significantly affect gaze direction and vestibulo-ocular compensation in this range. Moreover, control of head translation and orientation are probably inseparable in terms of the complex muscular physiology and joint interactions of the neck (Richmond and Vidal 1988). In particular, head translations probably also affect the translational locations of the rotational axes that we have described here (Melis 1996). Therefore in the future, it will be useful to place the relatively simple orientation constraints that we have described here into the broader context of controlling the head as a six degree-of-freedom rotational/translational body.

Implications for models and the physiology of head-free gaze control

The remarkable accuracy of the visual axis during large head-free saccades, despite variations in eye-head contribution (Becker and Jürgens 1992; Freedman and Sparks 1997; Fuller 1996; Guitton and Volle 1987) and perturbations to the trajectory (Goffart et al. 1998a; Péllison et al. 1995; Tomlinson 1990), suggests the existence of a dynamic gaze error signal that guides and terminates the overall gaze shift (Galiana and Guitton 1992; Galiana et al. 1992; Goosens and Van Opstal 1997; Laurutis and Robinson 1986; Tomlinson and Bahra 1986). Although 3-D feedback is required to update gaze error for torsional and noncommutative motion (Henriques et al. 1998; Tweed 1997), the output signal is likely coded in two dimensions at the level of the cortex and colliculus (Van Opstal et al. 1991). However, the observed behavior of the primate suggests that this 2-D signal must be decomposed into control signals matched to the eye and head in a very complex fashion. For example, like others (as reviewed in Guitton 1992), we have observed that large self-paced gaze shifts are broken down into several interim Eh saccades and intervening slow phases. The utility of this strategy is clear: it allows the visual system to gather brief snapshots of useful information during the course of a relatively long-lasting gaze shift. However, it now requires the brain to simultaneously specify separate goals, one for the ultimate desired target and several simultaneous goals for the

[3] The greater variability of twist in the pin-hole goggle range of *animal M1* might be related to its tendency to more readily optimize rotation axes as seen during the repetitive task. If all axes are optimized to minimize the angle of rotation, Donders' law would break down (Tweed and Vilis 1990) and random range twists could appear, depending on the idiosyncratic paths of the head in the random task.

interim Eh saccades. Furthermore introspection seems to suggest that the ultimate goal can be chosen voluntarily, whereas the precise spatial pattern of the interim saccades probably is selected by mechanisms that are largely involuntarily.

A reasonable hypothesis to explain this behavior is that the interim saccades are generated by a quasi-independent brain stem circuit (Paré and Guitton 1998; Tomlinson and Brance 1992) that is nested within an overall gaze feedback loop that specifies the ultimate goal at the level of cortex and the superior colliculus (Galiana and Guitton 1992; Galiana et al. 1992; Goosens and Van Opstal 1997; Guitton et al. 1990; Tomlinson 1990). Because it has been suggested that visual representations are remapped in the cortex and colliculus during saccades to maintain spatial constancy (Duhamel et al. 1992; Goldberg and Bruce 1990; Henriques et al. 1998; Walker et al. 1995), dynamic gaze error may be considered to be a special case of this mechanism, wherein a particular selected target is tracked in 2-D until it is brought into the foveal zone of internal retinotopic maps (Munoz and Wurtz 1995; Munoz et al. 1991; Van Opstal et al. 1991). This signal thus could continue to trigger multiple-step saccades in the brain stem circuit (until gaze feedback has signaled that the ultimate goal has been reached) through a mechanism that then becomes refractory until the next slow phases centers Eh.

In this nested arrangement, the 2-D to 3-D transformation for Listing's law would need to occur in the brain stem loop that maps saturated estimates of desired target displacement onto the appropriate desired final Eh orientation (Guitton and Volle 1987; Tweed 1997). As argued above, this requires knowledge of current eye position and either an efferent copy of intended head movement or a vestibular-derived estimate thereof. The cortical/collicular drive alone is probably not sufficient to specify this information. However, the vestibular nuclei and interstitial nucleus of Cajal collectively possess a 3-D representation of current eye position, ample vestibular information, and neurons that produce bursts of action potentials during vestibular driven quick phases (Crawford et al. 1997; Fukushima and Fukushima 1992; Helmchen et al. 1996; Kitama et al. 1995). The cerebellum also possesses a rich variety of information relevant to this task with important 3-D connections to the brain stem saccade generator (Goffart et al. 1998a), including inputs that appear to be involved in correcting torsional violations of Listing's law (Van Opstal et al. 1996). These structures thus collectively could form a circuit that specifies subgoals of desired final Eh position in a distributed fashion (Crawford and Guitton 1997b). In such a nested, distributed system, it would not be surprising that the brain stem would possess gaze-related activity in some signals (e.g., Cullen and Guitton 1997; Cullen et al. 1993), while retaining the ability to dissociate the Eh trajectory from gaze error in the manner observed in several behavioral paradigms (e.g., Crawford and Guitton 1997b; Tweed et al. 1995). Moreover, this scheme predicts that (and thus might explain why) microstimulation of the colliculus produces near-constant gaze displacements with the head free but then produces position-dependent goal-directed saccades when the head is fixed[4] (e.g., Freedman et al. 1996; Paré and Guitton 1998).

In contrast to the saccades that we quantified in this study, it would appear that the head movement was triggered only by the ultimate goal because the head showed no sign of accelerating/decelerating to match the interim eye movements. Again the brainstem reticular formation is probably important for selecting head movement metrics for a given gaze error. This being the case, it may form part of the network that constitutes the Fick gimbal operator discussed earlier. Note however, that our data suggested that this operator does not function within any feedback loop (as described earlier). This has the remarkable implication that head motor error normally is selected at the beginning of gaze saccades in primates but thereafter operates independently from gaze-error feedback.[5] This is similar to the scheme proposed by Tweed (1997), wherein the head was triggered by gaze error but only the eye was in the dynamic gaze feedback loop.

At first glance, this seems to contradict the finding that cat head motion can be updated by gaze error feedback during large perturbations to the system (Péllison et al. 1995). Assuming that the same is true for primate head movements, these observations once again can be reconciled by proposing a nested arrangement: suppose that the Donders' operator for the head is nested within a dynamic gaze error loop but is only triggered by gaze error when the target (desired gaze in space) is outside of the allowable Eh fixation zone (described earlier) at the desired Hs position. In normal circumstances, this would result in only a single large head movement toward the target. However, a large head perturbation (or a change in the desired target) could take the head trajectory far enough from its optimal goal (as defined in the preceding text) for dynamic gaze error to reactivate the Donders' operator and compute a new head motor error command. The possible utility of this arrangement is that it provides some voluntary flexibility in the choice of head movement strategies, while simultaneously making use of the more nimble oculomotor system to make up for small

[4] This can be explained as follows. Assume that *1*) the colliculus encodes retinal error, i.e., desired gaze displacement, *2*) a brain stem circuit drives Eh to a final desired position that is matched to a desired head position, and *3*) to do this, the latter circuit uses feedback information about actual head movement to anticipate subsequent slow phases (Crawford and Guitton 1997b), as we have proposed. First, stimulation of the colliculus in a head-free animal should correctly activate the brain stem circuit and produce natural looking eye-head movements with only a mild position-dependent convergence in gaze. The latter effect can be explained simply on the basis of the inherent position dependence of retinal error (Crawford and Guitton 1997a; Klier and Crawford 1998). However, with the head fixed, initial Eh position would tend to fall outside of the normal orbital zone associated with that particular head position and gaze direction. When activated, the colliculus/brain stem circuit would ''attempt'' to shift gaze and center the eye toward the normal Eh zone for that target direction. Because the head cannot move and because head feedback would inform the system that no subsequent slow phase is coming, saccades would simply drive the eye toward the desired Eh position, producing the observed goal-directed behavior (Freedman et al. 1996; Paré and Guitton 1998). The absence of this phenomenon in some stimulation preparations probably corresponds to extensive head-fixed training.

[5] Note, however, that the head movement signal, either in the form of efference copy or vestibular re-afference, still would have to be fed back to the common gaze error signal to make maintain the spatial registry of visual targets (Henriques et al. 1998) and ensure that gaze gets onto the target (Péllison et al. 1995).

idiosyncracies or deviations in the head trajectory. In principle, this scheme is no different from the proposed nesting of the oculomotor circuit (Paré and Guitton 1998), except that the larger mechanical range of the head would make multiple-step head movements unnecessary for targets within the visual range. Thus quasi-independent 3-D eye- and head-control systems (nested within a dynamic feedback loop that drives 2-D gaze error) may be the optimal control solution for head-free gaze control in the primate.

APPENDIX

Algorithms for gaze velocity criteria

This section describes the algorithms (in generic code) and velocity criteria used to select Eh data at various phases in the gaze shift. Three-dimensional angular velocities of Es and Hs were computed as described earlier (Crawford and Vilis 1991), and their magnitudes (speed) were computed by taking the square root of the sum of squares of the components. The following four measures of speed are employed further in the following text, measured in degrees/second, as well as generic string variables H, G, and VOR.

S_H = current head speed; S_G = current gaze (Es) speed; S_H(next) = head speed over the subsequent data interval; S_G(next) = gaze speed over the subsequent data interval.

Fixation

If $S_H < 10°/s$ and $S_G < 10°/s$ then [analyze data].

Eh(head-free) saccade starts

If S_H(next) $< 10°/s$ then H = off. If S_H(next) $> 25°/s$ then H = on. If $S_G < (S_H + 50°/s)$ then G = off. If H = on and G = off and S_G(next) > 100 and S_G(next) $> S_H$ then: [G = on, analyze data.] End if.

Eh (head-free) saccade ends

If S_H(next) $< 10°/s$ then H = off. If S_H(next) $> 25°/s$ (or sometimes 150°/s) then H = on. If H = on and $S_G > (S_H + 100°/s)$ then G = on. If G = on and S_G(next) $< (S_H + 30°/s)$ then: [G = on, analyze data] End if.

Slow phase ends

If S_H(next) $> 25°/s$ and $S_G > (S_H + 100°/s)$ then G = on. If G = on and $S_H > 25°/s$ and $S_G < S_H/2$ then [VOR = on, G = off] End if. If VOR = on and S_H(next) $< 5°/s$ then [G = off, VOR = off, analyze data] End if. If VOR = on and S_H(next) $> (S_H + 50°/s)$ then [VOR = off, analyze data] End if. If S_G(next) $> S_H$ then G = on. If S_H(next) $< 5°/s$ then G = off.

J. D. Crawford thanks J. Roi, L. Volume, W. Lezama, and J. Laurence for technical assistance, Dr. D. Tweed for critical editorial comments, and S. N. for inspiration.

This work was funded by Canadian Medical Research Council grants to J. D. Crawford and D. Guitton and by the Human Frontiers Science Organization (D. Guitton). J. D. Crawford is an Alfred. P. Sloan Fellow and holds a Canadian Medical Research Council Scholarship.

Address for reprint requests: J. D. Crawford, Dept. of Psychology, York University, 4700 Keele St., Toronto, Ontario M3J 1P3, Canada.

Received 17 August 1998; accepted in final form 5 January 1999.

REFERENCES

ANGELAKI, D. E. AND HESS, B.J.M. Inertial representation of angular motion in the vestibular system of rhesus monkeys. II. An otolith-controlled transformation that depends on an intact cerebellar nodulus. *J. Neurophysiol.* 73: 1729–1751, 1995.

BECKER, W. AND JÜRGENS, R. Gaze saccades to visual targets: does head movement change the metrics? In: *The Head-Neck Sensory-Motor System,* edited by A. Berthoz, W. Graf, and P. P. Vidal. New York: Oxford Univ. Press, 1992, p. 427–433.

BIZZI, E., KALIL, R. E., AND TAGLIASCO, V. Eye-head coordination in monkeys: evidence for centrally patterned organization. *Science* 173: 452–454, 1971.

COLLEWIJN, H., VAN DER STEEN, J., FERMAN, L., AND JANSEN, T. C. Human ocular counterroll: assessment of static and dynamic properties from electromagnetic scleral coil recordings. *Exp. Brain Res.* 59: 185–196, 1985.

CRAWFORD, J. D. AND D. GUITTON. Motor adpaptation of 2-D and 3-D aspects of eye-head coordination in monkeys. *Soc. Neurosci. Abstr.* 21: 1271, 1995.

CRAWFORD, J. D. AND D. GUITTON. Visual-motor transformations required for accurate and kinematically correct saccades. *J. Neurophysiol.* 78: 1447–1467, 1997a.

CRAWFORD, J. D. AND GUITTON, D. Primate head-free saccade generator implements a desired (post-VOR) eye position command by anticipating intended head motion. *J. Neurophysiol.* 78: 2811–2816, 1997b.

CRAWFORD, J. D. AND VILIS, T. Axes of eye rotation and Listing's law during rotations of the head. *J. Neurophysiol.* 65: 407–423, 1991.

CRAWFORD, J. D. AND VILIS, T. How does the brain deal with the problems of rotational movement? *J. Mot. Behav.* 27: 89–99, 1995.

CRAWFORD, D., VILIS, T., AND CADERA, W. Quick phase planes anticipate violations of Listing's law produced by slow phases. *Soc. Neurosci. Abstr.* 15: 211.5, 1989.

CRAWFORD, J. D., VILIS, T., AND GUITTON, D. Neural coordinate systems for head-fixed and head-free gaze shifts. In: *Three-Dimensional Kinematic Principles of Eye, Head, and Limb Movements in Health and Disease,* edited by M. Fetter, H. Misslisch, and D. Tweed. Harwood: Amsterdam, 1997, p. 43–56.

CULLEN, K. E. AND GUITTON, D. An analysis of primate inhibitory burst neuron spike trains using system identification techniques. II. Relationship to gaze, eye, and head movement dynamics during head-free gaze shifts. *J. Neurophysiol.* 78: 3283–3306, 1997.

CULLEN, K. E., GUITTON, D., JIANG, W., AND REY, D. G. Gaze-related activity of putative inhibitory burst neurons in the head-free cat. *J. Neurophysiol.* 70: 2678–2683, 1993.

DEMER, J. L., MILLER, J. M., POUKENS, V., VINTERS, H. V., AND GLASGOW, B. J. Evidence for fibromuscular pulleys of the recti extraocular muscles. *Invest. Ophthal. Vis. Sci.* 36: 1125–1136, 1995.

DESOUZA, J.F.X, NICOLLE, D. A., AND VILIS, T. Task-dependent changes in the shpae and thinckness of Listing's plane. *Vision Res.* 37: 2271–2282, 1997.

DICHGANS, J., BIZZI, E., MORASSO, P. AND TAGLIASCO, V. Mechanisms underlying recovery of eye-head coordination following bilateral labyrinthectomy in monkeys. *Exp. Brain. Res.* 18: 548–562, 1973.

DONDERS, F. C. Bietrag zur Lehr von den Bewigungen des menschlichen Auges. *Holländ. Beit. Anatom. Physiolog. Wiss.* 1: 105–145, 1848.

DUHAMEL, J.-R., COLBY, C. L., AND GOLDBERG, M. E. The updating of the representation of visual space in parietal cortex by intended eye movements. *Science* 255: 90–92, 1992.

FERMAN, L., COLLEWIJN, H., AND VAN DEN BERG, A. V. A direct test of Listing's law. I. Human ocular torsion measured in static tertiary positions *Vision Res.* 27: 929–938, 1987a.

FERMAN, L., COLLEWIJN, H., AND VAN DEN BERG, A. V. A direct test of Listing's law. II. Human ocular torsion measured under dynamic conditions. *Vision Res.* 27: 939–951, 1987b.

FREEDMAN, E. G. AND SPARKS, D. L. Eye-head coordination during head unrestrained gaze shifts in rhesus monkeys. *J. Neurophysiol.* 77: 2328–2348, 1997.

FREEDMAN, E. G., STANFORD, T. R., AND SPARKS D. L. Combined eye-head gaze shifts produced by electrical stimulation of the superior colliculus in Rhesus monkeys. *J. Neurophysiol.* 76: 927–951, 1996.

FULLER, J. H. Eye position and target amplitude effects on human visual saccadic latencies. *Exp. Brain Res.* 109: 457–466, 1996.

FUKUSHIMA, K. AND FUKUSHIMA, J. The interstitial nucleus of Cajal is involved in generating downward fast eye movements in alert cats. *Neurosci. Res.* 15: 299–303, 1992.

GALIANA, H. L. AND GUITTON, D. Central organization and modelling of eye-head coordination during orienting gaze shifts. *Ann. NY Acad. Sci.* 565: 452–471, 1992.

GALIANA, H. L., GUITTON, D., AND MUNOZ, D. P. Modeling head-free gaze control in the cat. In: *The Head-Neck Sensory-Motor System,* edited by A.

Berthoz, W. Graf, and P. P. Vidal. New York: Oxford Univ. Press, 1992, p. 520–525.

GLENN, B. AND VILIS, T. Violations of Listing's law after large eye and head gaze shifts. *J. Neurophysiol.* 68: 309–317, 1992.

GOFFART, L., GUILLAUME, A. AND PÉLLISON, D. Compensation for gaze perturbation during inactivation of the caudal fastigial nucleus in the head-unrestrained cat. *J. Neurophysiol.* 80: 1552–1557, 1998a.

GOFFART, L., PÉLLISON, D., AND GUILLAUME, A. Orienting gaze shifts during muscimol inactivation of caudal fastigial nucleus in the cat. II. Dynamics and eye-head coupling. *J. Neurophysiol.* 79: 1959–1976, 1998b.

GOLDBERG, M. E. AND BRUCE, C. J. Primate frontal eye fields. III. Maintenance of a spatially accurate saccade signal. *J. Neurophsyiol.* 64: 489–508, 1990.

GOOSSENS, H.H.L.M. AND VAN OPSTAL, A. J. Human eye-head coordination in two dimensions under different sensorimotor conditions. *Exp. Brain Res.* 114: 542–560, 1997.

GUITTON, D. Control of eye-head coordination during orienting gaze shifts. *Trends Neurosci.* 15: 174–179, 1992.

GUITTON, D. AND CRAWFORD, J. D. Three-dimensional constraints on coordinated eye-head gaze shifts in the monkey. *Soc. Neurosci. Abstr.* 20: 1405, 1994.

GUITTON, D., MUNOZ, D. P., AND GALIANA, H. L. Gaze control in the cat: studies and modelling of the coupling between orienting eye and head movements in different behavioural tasks. *J. Neurophysiol.* 64: 509–531, 1990.

GUITTON, D. AND VOLLE, M. Gaze control in humans: eye-head coordination during orienting movements within and beyond the oculomotor range. *J. Neurophysiol.* 58: 427–459, 1987.

HASLWANTER, TH. Mathematics of three-dimensional eye rotations. *Vision Res.* 35: 1727–1739, 1995.

HASLWANTER, T., CURTHOYS, I. S., BLACK, R. A., TOPPLE, A. N., AND HALMAGYI, G. M. The three-dimensional human vestibular-ocular reflex; response to long-duration yaw angular accelerations. *Exp. Brain Res.* 109: 303–311, 1995.

HAUSTEIN, W. AND MITTELSTAEDT, H. Evaluation of retinal orientation and gaze direction in the perception of the vertical. *Vision Res.* 30: 255–262, 1990.

HELMCHEN, C., RAMBOLD, AND BÜTTNER, U. Saccade-related burst neurons with torsional and vertical on-directions in the interstitial nucleus of Cajal in the alert monkey. *Exp. Brain Res.* 112: 63–78, 1996.

HENN, V., HEPP, K., AND VILIS, T. Rapid eye movement generation in the primate: physiology, pathophysiology, and clinical implications. *Rev. Neurol. Paris.* 145: 540–545, 1989.

HENRIQUES, D.Y.P., KLIER, E. M, SMITH, M. A., LOWY, D, AND CRAWFORD, J. D. Gaze-centered remapping of remembered visual space in an open-loop pointing task. *J. Neurosci.* 18: 1583–1594, 1998.

HERING, E. *Die Lehre vom Binokularin Sehen.* Leipzig: Engelmann, 1868.

HEPP, K. Oculomotor control: Listing's law and all that. *Curr. Opin. Neurobiol.* 4: 862–868, 1994.

HESS, B.J.M. AND ANGELAKI, D. E. Kinematic principles of primate rotational vestibulo-ocular reflex. I. spatial organization of fast phase velocity axes. *J. Neurophysiol.* 78: 2193–2202, 1997.

HOWARD, I. P. AND ZACHER, J. E. Human Cyclovergence a function of stimulus frequency and amplitude. *Exp. Brain Res.* 85: 445–450, 1991.

KITAMA, T., OHKI, Y., SHIMAZU, H., TANAKA, M., AND YOSHIDA, K. Site of interaction between saccade signals and vestibular signals induced by head rotation in the alert cat: functional properties and afferent organization of burster-driving neurons. *J. Neurophysiol.* 74: 273–287, 1995.

KLIER, E. M. AND CRAWFORD, J. D. The human oculomotor system accounts for 3-D eye orientation in the visual-motor transformation for saccades. *J. Neurophysiol.* 80: 2274–2294, 1998.

KLIER, E. M., GUITTON, D., AND CRAWFORD, J. D. Trajectories and 3-D fixation ranges of the eye and head during large gaze shifts in the monkey. *Soc. Neurosci. Abstr.* 24: 1743, 1998.

LAURUTIS, V. P. AND ROBINSON, D. A. The vestibulo-ocular reflex during human saccadic eye movements. *J. Physiol. (Lond.)* 373: 209–233, 1986.

MARR, D. *Vision: A Computational Investigation into the Human Representation and Processing of Visual Information.* San Francisco: Freeman, 1982.

MELIS, B.J.M. *Plasticity and Kinematic Constraints in 3-D Eye-Head Control* (PhD thesis). Nijmegen, The Netherlands: Universiteit Nijmegen, 1996.

MISSLISCH, H., TWEED, D., FETTER, M., SIEVERING, D., AND KOENIG, E. Rotational kinemtatics of the human vestibuloocular reflex. III. Listing's law. *J. Neurophysiol.* 72: 2490–2502, 1994a.

MISSLISCH, H., TWEED, D., FETTER, M., AND VILIS, T. The influence of gravity on Donders' law for head movements. *Vision. Res.* 34: 3017–3025, 1994b.

MISSLISCH, H., TWEED, D., AND VILIS, T. Neural constraints on eye motion in human eye-head saccades. *J. Neurophysiol.* 79: 859–869, 1998.

MUNOZ, D. P., GUITTON, D., AND PÉLLISSON, D. Control of orienting gaze shifts by the tecto-reticulo-spinal system in the cat whose head is unrestrained. III. Spatio-temporal characteristics of phasic motor discharges. *J. Neurophysiol.* 66: 1642–1666, 1991.

MUNOZ, D. P. AND WURTZ, R. H. Saccade-related activity in monkey superior colliculus. II. Spread of activity during saccades. *J. Neurophsyiol.* 73: 2313–2333, 1995.

OPTICAN, L. M. AND MILES, F. A. Visually induced adpative changes in primate saccadic oculomotor signals. *J. Neurophysiol.* 54: 940–958, 1985.

PARÉ, M. AND GUITTON, D. Brain stem omnipause neurons and the control of combined eye-head gaze saccades in the alert cat. *J. Neurophysiol.* 79: 3060–3076, 1998.

PÉLLISON, D., GUITTON, D., AND GOFFART, L. On-line compensation of gaze shifts perturbed by micro-stimulation of the superior colliculus in the cat with unrestrained head. *Exp. Brain Res.* 106: 196–204, 1995.

PÉLLISON, D., PRABLANC, C., AND URQUIZAR, C. Vestibulo-ocular reflex inhibition and gaze saccade control characteristics during eye-head coordination in humans. *J. Neurophysiol.* 59: 997–1013, 1988.

PHILIPS, J. O., LING, L., FUCHS, A. F., SIEBOLD, C., AND PLORDE, J. J. Rapid horizontal gaze movement in the monkey. *J. Neurophysiol.* 73: 1632–1652, 1995.

QUAIA, C. AND OPTICAN, L. M. Commutative saccadic generator is sufficient to control a 3-D ocular plant with pulleys. *J. Neurophysiol.* 79: 3197–3215.

RADAU, P., TWEED, D., AND VILIS, T. Three-dimensional eye, head, and chest orientations following large gaze shifts and the underlying neural strategies. *J. Neurophysiol.* 72: 2840–2852, 1994.

RAPHAN, T. Modelling control of eye orientation in three dimensions. In: *Three-Dimensional Kinematics of Eye, Head and Limb Movements,* edited by M. Fetter, T. Haslwanter, H. Misslisch, and D. Tweed. Amsterdam: Harwood, 1997, p. 359–374.

RAPHAN, T. Modelling control of eye orientation in three dimensions. I. Role of muscle pulleys in determining saccadic trajectory. *J. Neurophysiol.* 79: 2653–2667, 1998.

RICHMOND, F.J.R. AND VIDAL, P. P. The motor system: joints and muscles of the neck. In: *Control of Head Movement,* edited by B. W. Peterson and F. J. Richmond. New York: Oxford Univ. Press, 1988, p. 1–21.

ROBINSON, D. A. AND ZEE, D. S. Theoretical considerations of the function and circuitry of various rapid eye movements. In: *Progress in Oculomotor Research, Dev. Neurosci.,* edited by A. F. Fuchs and W. Becker. New York: Elsevier/North-Holland, 1981, vol. 12, p. 3–9.

SMITH, M. A. AND CRAWFORD, J. D. Neural control of rotational kinematics within realistic vestibulo-ocular coordinate systems. *J. Neurophysiol.* 80: 2295–2315, 1998.

STRAUMANN, D., HASLWANTER, TH., HEPP-REYMOND, M.-C., AND HEPP, K. Listing's law for the eye, head and arm movements and their synergistic control. *Exp. Brain Res.* 86: 209–215, 1991.

STRAUMANN, D., ZEE, D. S., SOLOMON, D., LASKER, A. G., AND ROBERTS, D. C. Transient torsion and cyclovergence during and after saccades. *Vision Res.* 35: 3321–3335, 1995.

TOMLINSON, R. D. Combined eye-head gaze shifts in the primate. III. Contribution to the accuracy of gaze saccades. *J. Neurophysiol.* 64: 1873–1891, 1990.

TOMLINSON, R. D. AND BAHRA, P. S. Combined eye-head gaze shifts in the primate. II. Interaction between saccades and the vestibuloocular reflex. *J. Neurophysiol.* 56: 1558–1570, 1986.

TOMLINSON, R. D. AND BRANCE, M. Brainstem control of coordinated eye-head gaze shifts. In: *The Head-Neck Sensory-Motor System,* edited by A. Berthoz, W. Graf, and P. P. Vidal. New York: Oxford Univ. Press, 1992, p. 356–361.

THEEUWEN M., MILLER, L. E., AND GIELEN, C.C.A.M. Is the orientation of head and arm coupled during pointing movements? *J. Motor Behav.* 25: 242–250, 1993.

TWEED, D. Three-dimensional model of the human eye-head saccadic system. *J. Neurophysiol.* 77: 654–666, 1997.

TWEED, D. CADERA, W., AND VILIS, T. Computing three-dimensional eye position quaternions and eye velocity from search coil signals. *Vision Res.* 30: 97–110, 1990.

TWEED, D., GLENN, B., AND VILIS, T. Eye-head coordination during large gaze shifts. *J. Neurophysiol.* 73: 766–779, 1995.

TWEED D., MISSLISCH H., AND FETTER M. Testing models of the oculomotor velocity to position transformation. *J. Neurophysiol.* 72: 1425–1429, 1994.

TWEED, D. AND VILIS, T. Geometric relations of eye position and velocity vectors during saccades. *Vision Res.* 30: 111–127, 1990a.

TWEED, D. AND VILIS, T. Listing's law for gaze-directing head movements. In: *The Head-Neck Sensory-Motor System*, edited by A. Berthoz, W. Graf, and P. P. Vidal. New York: Oxford Univ. Press, 1992, p. 387–391.

VAN OPSTAL, A. J., HEPP, K., HESS, B.J.M., STRAUMANN, D., AND HENN, V. Two- rather than three-dimensional representation of saccades in monkey superior colliculus. *Science* 252: 1313–1315, 1991.

VAN OPSTAL, A. J., HEPP, K., SUZUKI, Y., AND HENN, V. Role of monkey nucleus reticularis tegmenti pontis in the stabilization of Listing's plane. *J. Neurosci.* 16: 7284–7296, 1996.

VON HELMHOLTZ, H. *Treatise on Physiological Optics (English Translation)*, translated by J.P.C. Southall. Rochester, NY: Optical Society of America, 1925, vol. 3, p. 44–51.

WADE, S. W. AND CURTHOYS, I. S. The effect of ocular torsional position on perception of the roll-tilt of visual stimuli. *Vision Res.* 37: 1071–1078, 1997.

WALKER, M. F., FITZGIBBON, J., AND GOLDBERG, M. E. Neurons of the monkey superior colliculus predict the visual result of impeding saccadic eye movements. *J. Neurophysiol.* 73: 1988–2003, 1995.

WESTHEIMER, G. Kinematics of the eye. *J. Opt. Soc. Am.* 47: 967–974, 1957.